UCLA

Structural & Geotechnical Engineering Laboratory

LABORATORY EVALUATION OF SEISMIC FAILURE MECHANISMS OF LEVEES ON PEAT

Jonathan P. Stewart, PhD, PE (PI)
Scott J. Brandenberg, PhD (Co PI)
Ali Shafiee
Department of Civil and Environmental Engineering
University of California, Los Angeles

A report on research conducted under Grant No. G11AP20169 from the
U.S. Geological Survey, National Earthquake Hazards Reduction Program.

Report UCLA-SGEL 2013/04
Structural and Geotechnical Engineering Laboratory
Department of Civil & Environmental Engineering
University of California, Los Angeles

September 2013

UCLA - SGEL

Report 2013/04

Laboratory Evaluation of Seismic Failure Mechanisms of Levees on Peat

Jonathan P. Stewart, PhD, PE (PI)
Scott J. Brandenberg, PhD (Co PI)
Ali Shafiee

Department of Civil and Environmental Engineering
University of California, Los Angeles

A report on research conducted under Grant No. G11AP20169 from the
U.S. Geological Survey, National Earthquake Hazards Reduction Program.

Report UCLA-SGEL 2013/04
Structural and Geotechnical Engineering Laboratory
Department of Civil & Environmental Engineering
University of California, Los Angeles

September 2013

ABSTRACT

USGS/NEHRP Award No. G11AP20169

LABORATORY EVALUATION OF SEISMIC FAILURE MECHANISMS OF LEVEES ON PEAT

PI: Jonathan P. Stewart, Co PI: Scott J. Brandenberg
Civil & Environmental Engineering Department
University of California
Los Angeles, CA 90095-1593
Tel: (310) 206-2990 Fax: (310) 206-2222
jstewart@seas.ucla.edu; sjbrandenberg@ucla.edu

Many of the levees in the Sacramento-San Joaquin Delta are founded on peaty organic soils. The operating assumption in previous studies of the vulnerability of Delta levees to earthquakes is that the only possible failure mechanisms are those associated (1) with soil liquefaction and related strength loss and (2) for nonliquefiable soils (such as peats), shear failure under dynamic loads that induce landslide-type displacements. Under this set of assumptions, the risk to Delta levees is dominated by liquefaction, with the very soft peaty soils that underlie much of the levee system playing no significant role in ground failure, although the peat does alter the ground motion due to site response. This project is intended to challenge the fundamental assumptions of that prior work by examining the behavior of peaty organic soil during and following strong cyclic loading, such as would occur during earthquakes. This examination of the peat soil behavior is undertaken with a program of laboratory testing.

An initial component of this project was to upgrade a simple shear testing device to enable constant volume testing. We then use this device and other devices for testing of peaty organic soils to investigate their tendency to develop pore pressures during cyclic loading and the effect of the pore pressure generation on shear strength and post-cyclic volume change. We have adapted an existing state-of-the-art digitally controlled simple shear device, originally designed for drained testing, to perform constant height testing. The new system utilizes PID control of horizontal displacements coupled with either vertical force control or vertical displacement control. We show that the level of vertical control achieved during constant-height testing is excellent in several respects – the levels of height change are very small (less than 0.05% of the specimen height for large shear-strain tests) and are maintained even at relatively high frequencies. This level of vertical control, especially at high frequencies, has not been possible in prior simple shear devices. Moreover, rocking of the top cap is shown to be similarly small, with the height change due to rocking at the specimen edge being half or less than that associated with vertical control. To our knowledge, this is the first such documentation of device performance with respect to rocking.

We investigated through laboratory testing the volume change characteristics of peaty organic soil from Sherman Island, California under static conditions and under cyclic and post-cyclic conditions from cyclic triaxial (CTX) and cyclic direct simple shear (DSS) testing. Incremental consolidation tests indicate the material to be highly compressible ($0.8<C_c<6.8$, $0.05<C_r<0.8=0.4$) and prone to substantial ageing from secondary compression. Careful examination of the consolidation test data shows an important, and rather fundamental, aspect of secondary compression, which is that its characteristic feature of occurring at an exponentially decaying rate following load application is not universal. Rather, that "classical" behavior occurs only following stages of loading that produce at least 3.0% vertical strain. On the other hand, for smaller load increments, the secondary compression rate following the addition of load is relatively modest, and in the extreme may not depart from what occurred prior to load application. We proposed a simple model to characterize this effect that is based on inference of a 'resetting' time for secondary compression. To our knowledge, this report presents the first ever concept of the 'resetting' time, which we believe to be a fundamental feature of secondary compression.

From strain-controlled cyclic triaxial and simple shear testing of peaty organic soil from Sherman Island, we find the generation of cyclic pore pressures to increase markedly for cyclic shear strain levels beyond approximately 0.5-1.0%, with the largest residual pore pressure ratios r_{ur} (cyclic residual pore pressure normalized by pre-cyclic consolidation stress) being approximately 0.6-0.8 for DSS testing and 0.2-0.4 for CTX testing. For a given level of shear strain, we find larger pore pressures from DSS testing than for CTX testing. Post-cyclic volume change occurs from pore pressure dissipation and secondary compression. The level of post-cyclic primary consolidation appears to be uniquely related to the recompression index of the soil and r_{ur}. The secondary compression following cyclic loading is well explained by the proposed resetting model. Significantly, this work shows that when large cyclic shear strains occur in peaty organic soil, they cause pore pressure ratios that are not large enough to significantly degrade shear strength, but which are large enough to partially re-set the secondary compression process. This enhancement of secondary compression, in turn, could lead to settlements of levees founded on such materials that could produce catastrophic loss of freeboard if not mitigated. These possible failure mechanisms are not considered in existing hazard assessments for regions such as the California Bay-Delta region, and will need to be explored in future work.

ACKNOWLEDGMENTS

Support for this work was provided by the U.S. Geological Survey (USGS), Department of interior, under USGS Award No. G11AP20169. The views and conclusions contained in this document are those of the authors and should not be interpreted as necessarily representing official policies, either expressed or implied, of the U.S. Government.

TABLE OFCONTENTS

ABSTRACT ..... **ii**

ACKNOWLEDGMENTS ..... **iv**

TABLE OF CONTENTS ..... **v**

LIST OF FIGURES ..... **vii**

LIST OF TABLES ..... **x**

1 INTRODUCTION **1**

1.1 Background and Motivation **1**

1.2 Can Ground Failure in Peat Threaten Levees? **2**

1.3 Project Scope and Report Organization **3**

2 ADAPTATION OF DIGITALLY CONTROLLED SIMPLE SHEAR DEVICE FOR CONSTANT VOLUME TESTING **5**

2.1 Introduction **5**

2.2 UCLA DC-SS Device **7**

2.3 Upgrade for Constant Volume Testing **8**

2.3.1 Background on constant volume approach for undrained testing 8
2.3.2 UCLA DC-SS modification for constant volume testing 9

2.4 System Performance **11**

2.4.1 Horizontal axes performance 12
2.4.2 Vertical axis performance 16
2.4.3 Rocking 19

2.5 Calibration Tests **21**

2.5.1 Seismic compression of Silica No. 2 dry sand 21
2.5.2 Cyclic behavior of Silica No. 2 sand under constant-height conditions 24
2.5.3 Monotonic behavior of Flint No. 16 dry sand under constant-height conditions 25
2.5.4 Monotonic behavior of a normally consolidated clay under constant-height conditions 27

3 MECHANICAL BEHAVIOR OF SHERMAN ISLAND PEAT 29

3.1 Introduction 29

3.2 Site Characteristics and Sampling Technique 30

3.3 Tested Material and Procedure 31

3.4 Static Compressibility of Peat 33

3.5 Coefficient of Secondary Compression 35

3.5.1 Development of a new consolidometer to permit pore pressure measurement for determining t_p 36
3.5.2 Summary of consolidation tests performed using new consolidometer 38
3.5.3 Measured values of secondary compression index c_α 39
3.5.4 Interpreting the resetting of secondary compression clock 40

3.6 Cyclic Shear Testing of Peat Specimens 45

3.6.1 Test results 45
3.6.2 Resetting of secondary compression clock due to cyclic shearing 51

3.7 Implications of Secondary Compression Clock Resetting for Levees Founded on Peat 53

4 SUMMARY AND FUTURE WORK 54

4.1 Summary 54

4.2 Future Work 56

REFERENCES 59

LIST OF FIGURES

Figure 1.1 Waterways in the Sacramento – San Joaquin Delta (CDWR 1992). 1

Figure 1.2 Mechanisms of levee deformation by (a) deviatoric slumping and spreading and volumetric strain, (b) sliding due to failure along the base of the levee, and (c) bearing failure through the foundation soils.. 2

Figure 2.1 How simple shear testing simulates ground deformationd from vertically propagating shear waves (Chu-Chang 2002). 6

Figure 2.2 Cambridge versus NGI direct simple shear device (Franke et al. 1979) 6

Figure 2.3 Photograph showing (a) overview of device (b) close-up view of tri-post frame (c) view of specimen along with top and bottom caps with wire-reinforced membrane 7

Figure 2.4 Shematic configuration of the elements of the UCLA DC-SS constant height control system. 10

Figure 2.5 Sinusoid tracking of a cyclic displacement amplitude=0.01 mm for shearing along one axis at a time (a) command versus feedback signal, (b) evaluation of A/D performance, (c) FFT of the signals and noise. 13

Figure 2.6 Variation of tracking error for unidirectional shaking with (a) displacement amplitude and (b) command frequency from present study using PID control and Duku et al. (2007) using MIMO control. 14

Figure 2.7 Normalized root mean square of tracking errors on baseline axis for varying frequencies of excitation on perpendicular axis under present configuration using PID control and Duku et al. (2007) using MIMO control. 15

Figure 2.8 Effect of amplifying feedback signal prior to A/D conversion on the normalized root mean square error for harmonic excitation at (a)1.0 Hz and (b) 0.1 Hz. 16

Figure 2.9 Constant height strain-controlled test on Silica No.2 dry sand under an initial vertical stress (σ'_{v0}) of 100 kPa, and a frequency of 0.1 Hz 17

Figure 2.10 Performance of vertical axis in maintaining constant height condition 18

Figure 2.11 Performance of the UCLA DC-SS device in restraining rocking (1) angular distortions in a cyclic strain-controlled test (2) error term related to the vertical deformation caused by rocking. 21

Figure 2.12 Cyclic strain-controlled simple shear test results on a dry sand (Silica No.2, D_r=45%) 22

Figure 2.13 Performance of the new control system in terms of seismic compression of Silica No. 2 sand. 23

Figure 2.14 Cyclic behavior of Silica No.2 dry sand under constant volume conditions at different densities. 26

Figure 2.15 Monotonic undrianed behavior of Flint No. 16 dry sand under constant volume conditions at D_r=18%. 26

Figure 2.16 Monotonic behavior of a low plastic normally consolidated clay under constant volume conditions. 28

Figure 3.1 CPT tip resistance (q_c), and shear wave velocity (V_s) from a free-field site on Sherman Island (V_s profile from GeoVision 2000). 31

Figure 3.2 Typical settlement-time plots for an increment of load applied to peat. Specimen 8-3b, final σ'_{vc} =195 kPa. 34

Figure 3.3 Consolidation behavior of the tested peat (a) loading-reloading sequences for the specimen 8-3b (b) Variation of Cc and Cr with organic content for the Sherman Island peat. 35

Figure 3.4 Single-drainage consolidometer that permits pore pressure measurement at bottom of specimen. 37

Figure 3.5 Sample data from consolidation device in Fig. 3.4 that clearly shows why pore pressure measurement is necessary for determining end of primary consolidation. 38

Figure 3.6 Consolidation curve showing e vs. σ'_{vc}, and relation between secondary compression index and σ'_{vc} 40

Figure 3.7 Consolidation test on peat specimen with 51% organic content. In Stage 1, a vertical load increment of 9.3 kPa was imposed on an initially unloaded specimen, and in Stage 2, an additional 0.2 kPa load increment was imposed.. ...41

Figure 3.8 Void ratio versus time for the Stage 2 data plotted in Fig. 3.7, except with the clock reset at the time of application of the 0.2 kPa load increment.. 42

Figure 3.9 Void ratio versus time for the Stage 2 data plotted in Fig. 3.7, except with the clock reset at the time of application of the 0.2 kPa load increment. 43

Figure 3.10 Void ratio versus time for (a) Test 1, and (b) test 2. 44

Figure 3.11 Secondary compression reset index, θ, versus volumetric strain induced by primary consolidation, ε_{vc}.. 45

Figure 3.12 Cyclic behavior of a reconstituted specimen (organic content=51%) under cyclic loading in UCLA-DSS device. 47

Figure 3.13 Cyclic behavior of specimen 9-3a under cyclic loading in CTX device....48

Figure 3.14 Post-cyclic behavior of the tested peat (a) residual pore pressure, and (b) post-cyclic volume change at end of primary consolidation (t_p).. 49

Figure 3.15 Post-cyclic volume change from primary consolidation. 50

Figure 3.16 Post-cyclic volume change for a DSS test conducted on a reconstituted specimen (organic content=51%), $\sigma'_{vc} = 15kPa$ (a) $\gamma_c = 0.03\%$ (b) $\gamma_c = 3\%$ 51

Figure 3.17 Reset index for a DSS test conducted on a reconstituted specimen (organic content=51%), $\sigma'_{vc} = 15kPa$ in terms of (a) cyclic shear strain amplitude (b) residual pore pressure ratio (c) post-cyclic volume change from primary consolidation. 52

Figure 3.18 Post-cyclic index for a DSS test conducted on a reconstituted specimen (organic content=51%), $\sigma'_{vc} = 15kPa$ in terms of (a) cyclic shear strain amplitude (b) residual pore pressure ratio (c) total post-cyclic volume creep 53

LIST OF TABLES

Table 3.1 Testing for undisturbed and bulk samples taken from a depth of 1.3-3.0 m. 32

Table 3.2 Summary of consolidation tests perfromed using new consolidation device. 39

1 Introduction

1.1 BACKGROUND AND MOTIVATION

The Sacramento-San Joaquin Delta consists of more than 60 islands (Fig. 1.1) that are mostly below sea level, and protected by more than 1700 km of levees that constantly impound water. Delta levees are composed of poorly compacted sands, silts, clays, and organics often founded atop a thick layer of peaty organic soil. The stability of these levees is of great importance, since inundation of any of the major islands can draw saline water from the San Francisco Bay into the Delta, halting water exports to the central valley and southern California.

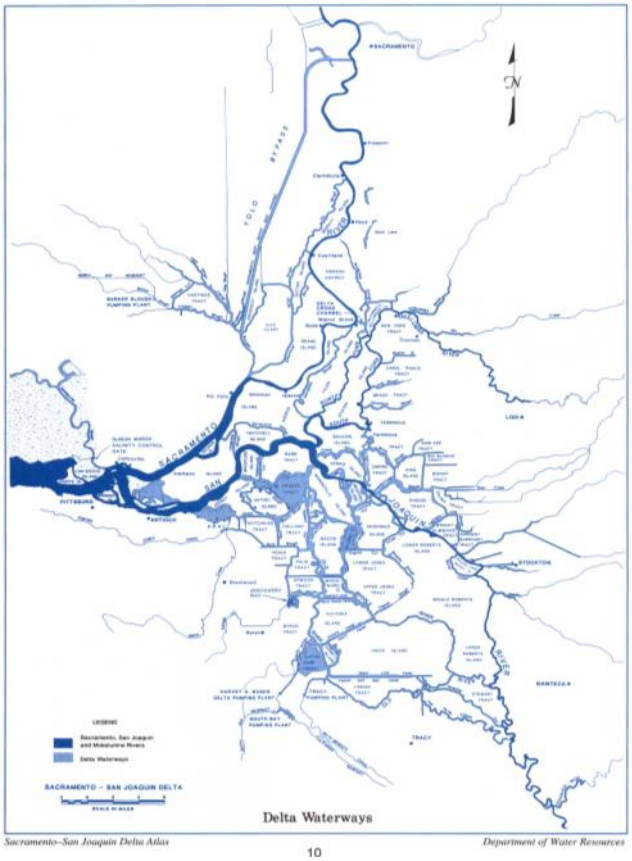

Figure 1.1. Waterways in the Sacramento - San Joaquin Delta (CDWR 1992).

The State of California sponsored the Delta Risk Management Strategy (DRMS) to quantify seismic risk and flood risk in the Delta using the best information currently available. Peak horizontal ground accelerations with a return period of 500 years approach 0.4g for soil conditions consistent with Pleistocene soils that underlie the peat (DRMS 2009). Using analysis procedures that largely neglect the potential for ground failure in peat, instead focusing on liquefaction and associated instabilities from strength loss in saturated sands, DRMS found that the 500 year shaking levels would be expected to cause 10 to 70 failures of the existing levees in a single earthquake. Various mitigation measures are

currently being considered to address this risk. The motivation for this report, in broad terms, is to challenge the assumption that the peaty organic soil is not a potentially significant contributor to seismic ground failure beneath the Delta levees.

1.2 CAN GROUND FAILURE IN PEAT THREATEN LEVEES?

The motivation for the present study was to answer the question in the section heading. As shown in Figure 1.2, we can envision several potential failure mechanisms for levees founded on peat that experience strong ground motion. Among the mechanisms that are depicted, we consider levee settlement due to volumetric and/or deviatoric straining in peaty foundation soils to be the most viable. Such settlement would be brought on by cyclic pore pressure generation and associated reconsolidation and softening. This mechanism was not considered in the DRMS (2009) study for good reason – it was not recognized and there is no analytical approach for doing so.

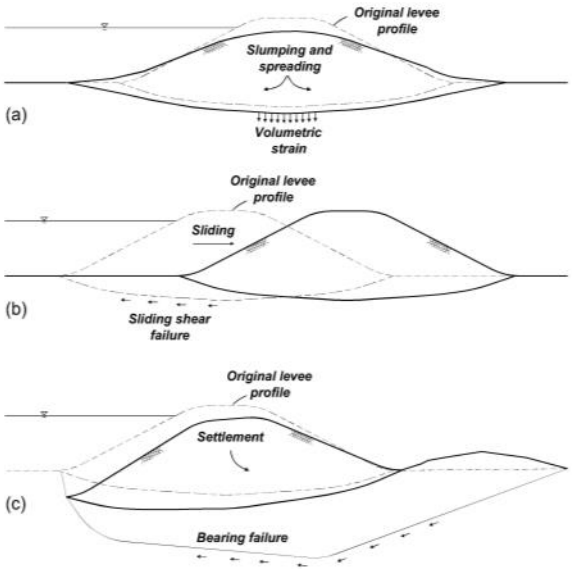

Figure 1.2. Mechanisms of levee deformation by (a) deviatoric slumping and spreading and volumetric strain, (b) sliding due to failure along the base of the levee, and (c) bearing failure through the foundation soils.

To provide context for understanding the value of our study, it must be recognized that current practice requires categorizing levee sites as being either potentially liquefiable or non-liquefiable, as done in the DRMS study. Liquefiable soils are known from extensive prior research to potentially exhibit significant strength loss that can lead to levee instability during earthquakes, and control 90% of the levee hazards identified in the DRMS study. Non-liquefiable soils do not exhibit significant strength loss during undrained shearing (*undrained* means that the soil is sheared at constant volume, without water leaving or entering the void space) and current analyses show that such materials will relatively rarely cause levee failures. Peats fall under the 'non-liquefiable' category and hence do not significantly contribute to current assessments of seismic risk in the Delta. Therein lies the problem – peats are highly

unusual soils that may pose problems that are not issues for traditional non-liquefiable soils such as clays and plastic silts. We contend that a better understanding of peat is needed to adequately evaluate the seismic risk to levees founded on these materials.

Peat is more pervasive than liquefiable sand in the Delta, but much less is known about its seismic behavior. Deformations of levees on non-liquefiable soils (including peat) were estimated in the DRMS study using Newmark sliding block analysis. The Newmark approach assumes sliding along a distinct failure surface of a rigid mass of soil, but its applicability to problems involving levees on highly deformable peaty organic soils is unknown. Typically, yield acceleration (an important input for the Newmark approach) is estimated using limit equilibrium analysis methods that assume soil behavior is rigid until the point of failure (i.e., rigid-plastic), and then forms a distinct failure surface along which shear strength is fully-mobilized. However, the peat soils in the Delta are among the softest in the world, and are therefore far from being rigid prior to failure. The extremely soft peat materials would be very unlikely to exhibit distinct rupture surfaces, and therefore limit equilibrium analysis methods are clearly inappropriate. Using limit equilibrium methods, the DRMS study predicted < 10% of the levee failures would be associated with non-liquefiable soils, including peat.

1.3 PROJECT SCOPE AND REPORT ORGANIZATION

The principal scope of this project was to (1) perform a series of monotonic, cyclic and dynamic tests on consolidated specimens of peaty organic soil to evaluate factors affecting pore pressure generation and its effects on post-cyclic re-consolidation and strength degradation; and (2) derive from those data preliminary relationships for evaluation of excess pore pressure build-up and post-cyclic volume change that are amenable for application in engineering design practice. It is understood that these relationships are material-specific and as such may not be applicable outside of the Delta region.

A practical hurdle that we faced in completing this scope was that the simple shear testing device required for the work initially lacked the capability for undrained cyclic shearing. Accordingly, prior to the onset of the project, and continuing during the initial portion of the project period, we undertook a substantial effort to upgrade the simple shear test device to enable

testing of the sort required by the project. While these upgrades were funded from other (private) sources, these device updates are important and are described within this report.

Following this introduction, we describe in Chapter 2 the aforementioned simple shear device and its recently completed upgrades. In Chapter 3 we describe the principal results of the cyclic and monotonic testing of selected peat materials using both cyclic triaxial and simple shear devices. Included within each chapter is a synthesis of directly related literature in order to place the contributions of the work in proper context.

2 Adaptation of Digitally Controlled Simple Shear Device for Constant Volume Testing

2.1 INTRODUCTION

Simple shear test apparatuses are often preferred for cyclic testing of soils because, as shown in Figure 2.1, the deformations imposed on test specimens mimic the effects of vertical one-dimensional shear wave propagation under in situ conditions. Conventional simple shear test apparatuses apply shear demands on specimens in a single horizontal direction and generally conform to one of the following configurations: (1) the Roscoe- or Cambridge-type apparatus in which cubical specimens are sheared on all four sides using hinged metallic walls (Figure 2.2a); or (2) the NGI-type apparatus (Kjellman 1951, Rosco 1953, Bjerrum and Landva 1966) in which short circular specimens are laterally confined by wire-reinforced membranes and shear stresses are applied on the top and base horizontal planes (Figure 2.2b). NGI-type apparatuses are particularly useful in engineering practice as they are well suited for the mounting and testing of relatively undisturbed field specimens, which are typically circular in shape.

This chapter describes modifications that were made to an NGI-type digitally controlled simple shear device previously developed at UCLA (referred to as the UCLA DC-SS device) by Duku et al. (2007). The following section reviews the principal attributes of this device and its unique attributes and capabilities relative to other simple shear devices used in research and practice. The principal limitation of this device is that the control system had not been configured to enable constant volume testing, which mimics undrained shear conditions in soil specimens. Accordingly, in the main body of this chapter, we describe modifications to the device to enable constant volume testing and describe a sequence of tests used to verify the reliability of the results obtained with the reconfigured system.

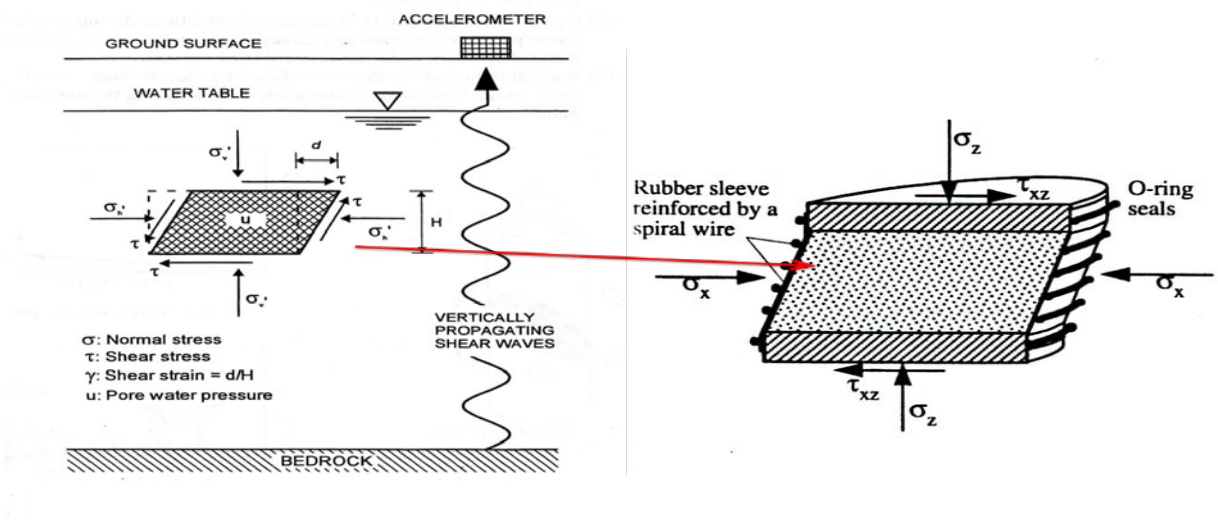

Figure 2.1. How simple shear testing simulates ground deformations from vertically propagating shear waves (Chu-Chang 2002)

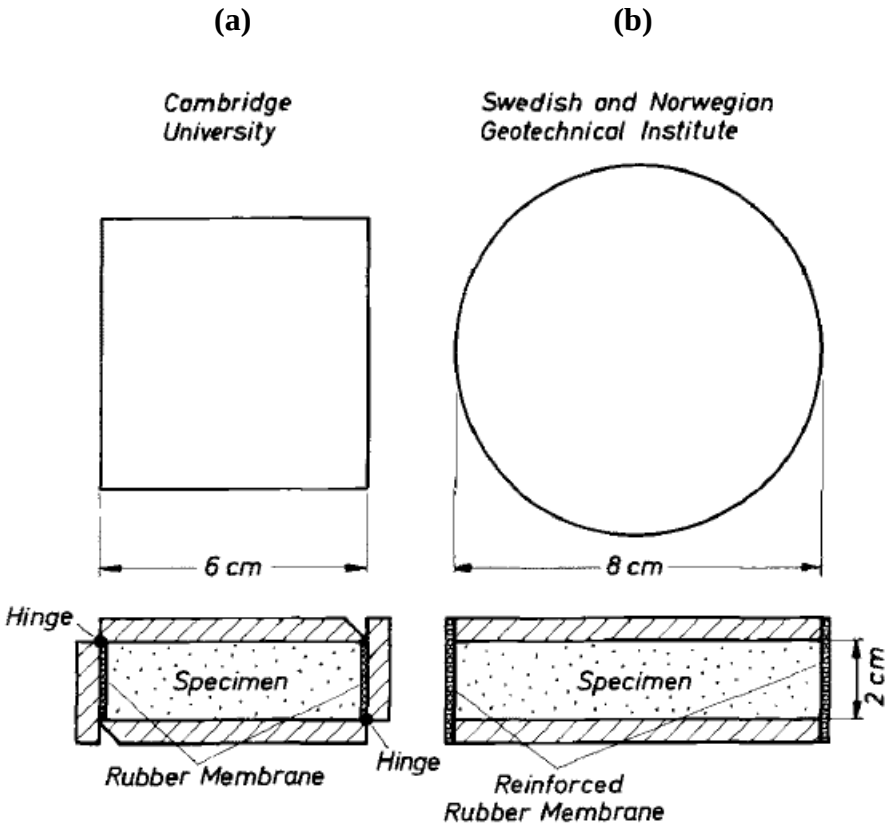

Figure 2.2. Cambridge versus NGI-type direct simple shear device (Franke et al. 1979)

2.2 UCLA DC-SS DEVICE

The UCLA DC-SS device is a digitally-controlled NGI-type simple shear device with capabilities for broadband multidirectional excitation. A device photograph is shown in Figure 2.3a. Duku et al. (2007) describe the device and its unique attributes relative to other research-level devices in the literature. Those unique attributes include the following: (1) it operates with servo-hydraulic actuators that can reproduce broadband (earthquake-like) excitation with relatively precise control as a result of device-specific true digital control algorithms; (2) it can shear soil specimens simultaneously in two horizontal directions with minimal cross coupling between the horizontal motions to more realistically simulate field stress paths; and (3) it has a stiff frame (Fig. 2.3b) and high performance track bearing that minimizes (but does not eliminate) system compliance associated with top cap rocking. The bottom cap is free to displace horizontally in two perpendicular directions (i.e., u_x and u_y) but cannot displace vertically. The top cap is fixed against horizontal movement but has the freedom to move vertically (i.e., u_z unless restrained by the control system). Vertical loads (F_z) are applied by the actuator visible in Figure 2.3a atop the frame; the loads are applied to the top cap.

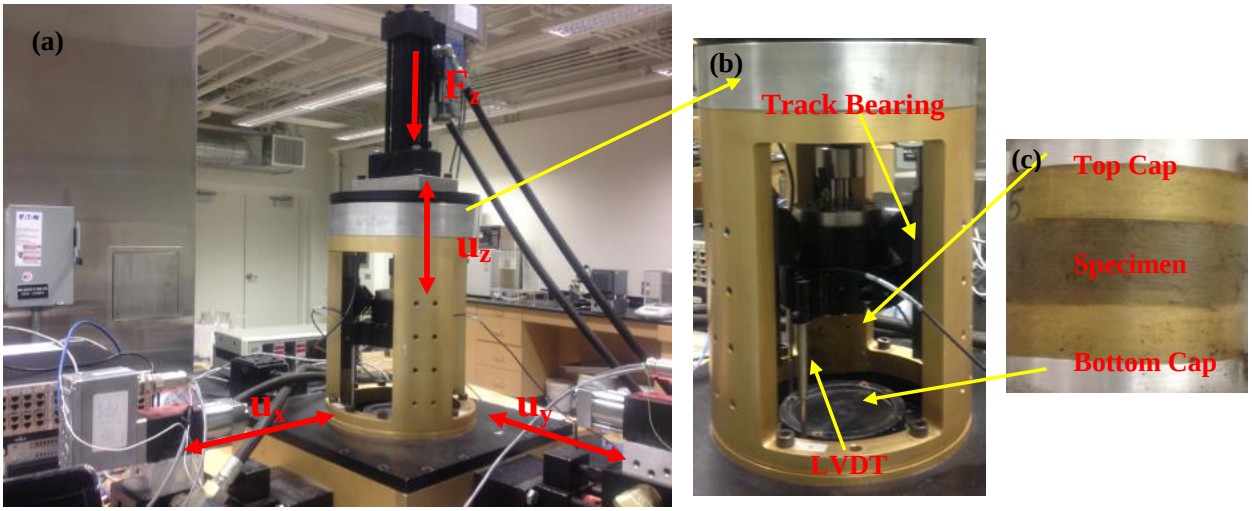

Figure 2.3. Photograph showing (a) Overview of device (b) close-up view of tri-post frame, (c) view of specimen along with top and bottom caps with wire-reinforced membrane

The UCLA DC-SS device was designed to test cylindrical soil specimens with a diameter of 10.2 cm or less. The specimen is located between relatively rigid bottom and top caps (Fig. 2.3c)

and is typically confined by a wire reinforced membrane. Once the specimen is secured between the two adapter plates, three LVDTs equally spaced around the specimen are mounted on the top adapter plate and fixed to the plate by set screws. The specimen is then consolidated by a vertical stress and is ready for shearing. At the 10.2 cm diameter and a typical height of 2.5 cm, the specimen aspect ratio is approximately 4:1, which Shen et al. (1978) have shown to produce nearly true simple shear conditions over most of the specimen cross-section despite the lack of complimentary shear stresses on vertical faces (i.e., at the membrane-soil interface).

The UCLA DC-SS device was original developed for relatively large-strain applications including seismic compression and shear strength (e.g., Duku et al., 2008; Yee et al., 2013). The original operational strain range was approximately cyclic shear strains (γ_c) of 0.1% and larger. Yee et al. (2011) extended its low strain capabilities by characterizing noisy signals and utilizing several statistical methods to extract meaningful responses for shear strains as low as approximately 0.03%.

2.3 UPGRADE FOR CONSTANT VOLUME TESTING

2.3.1 Background on constant volume approach for undrained testing

Prior to the present work, the UCLA DC-SS device was configured to maintain (nearly) constant vertical load, while allowing the top cap to displace vertically. As such, it was capable of simulating drained or partially drained conditions, but not undrained conditions in which no specimen volume change is allowed. True undrained shear is commonly applied in triaxial devices by applying specified external loads on saturated specimens while measuring pore pressures using transducers hydraulically connected to the specimen pore fluid via a porous stone in the specimen end cap. A critical detail in this testing is ensuring saturation through back-pressure saturation (Lowe and Johnson, 1960), so that contractive or dilatant soil behavior is reflected through pore pressure change and not volume change.

This testing approach, while common for triaxial shear, is typically not practical for simple shear because most devices are not configured to apply external cell pressures needed for back-pressure saturation. For this reason, alternative approaches have been developed in which unsaturated specimens are used and the device is configured to maintain constant specimen volume by varying external vertical loads during shear. The underlying assumption is that the

change in applied vertical stress as the specimen volume is maintained constant during shear is equal to the excess pore pressure that would have been measured in a truly undrained test (Bjerrum and Landva, 1966). This principal has previously been implemented in a Roscoe-type apparatus with constant total vertical stress by maintaining the boundary conditions of constant height and zero lateral strain (Vaid and Finn, 1979).

For NGI-type devices, application of the same principles is referred to as “constant height” testing because lateral boundary conditions are not controlled as part of the test aside from the use of wire-reinforced membranes. Such testing has been performed to investigate cyclic undrained behavior of sands with regard to liquefaction and cyclic degradation (e.g., Ishihara and Yamazaki 1980, Tatsuoka and Silver 1981) and undrained shear strength of clays (e.g., Hanzawa et al. 2007, Bro et al. 2013).

The veracity of the constant volume (or constant height) approach is well established from an experimental basis (Dyvik et al., 1987). This was demonstrated by Dyvik et al. (1987) by performing both true undrained simple shear testing, with constant load and pore pressure measurements, and by constant volume simple shear testing on similar specimens of normally consolidated clay. The stress–strain and stress path plots obtained by the two test types were nearly identical, thus indicating that the changes in vertical stress required to maintain constant volume are equivalent to the measured pore pressures in an undrained test.

2.3.2 UCLA DC-SS modification for constant volume testing

Some prior simple shear devices configured for constant volume testing have maintained height control mechanically, typically by clamping top and bottom caps against vertical displacement (e.g., Finn and Vaid 1977, Ishihara and Yamazaki 1980, Wijewickreme 2010). Others have used a control algorithm to adjust the vertical force using a servo-pneumatic actuator (e.g., Degroot et al. 1991) or electro-mechanical step motor (e.g., Porcino et al. 2006). We adopt the second approach but with a servo-hydraulic vertical actuator. This was accomplished by equipping the vertical axis with a servo electric valve, an actuator, and a load cell. A closed-loop control system (Fig. 2.4) was designed so that the feedback from vertical LVDTs are read and if they are not zero, the vertical load is adjusted to return the vertical displacement to zero. The advantage of servo-hydraulic control systems over other systems is that they are more responsive than

pneumatic systems when loading involves high-frequencies of up to 20 Hz. Prior control-based systems are reliable only for frequencies less than 1 Hz (e.g., Porcio et al. 2006).

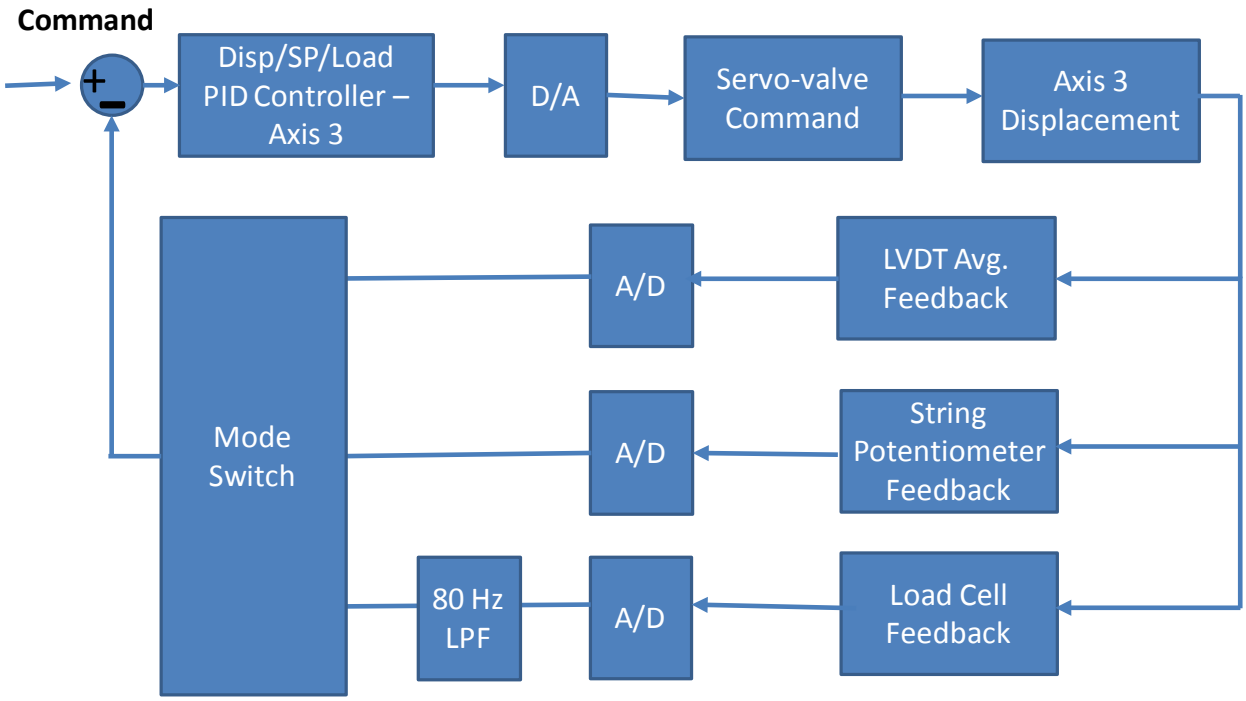

Figure 2.4. Schematic configuration of the elements of the UCLA DC-SS constant height control system

The control system of the device was upgraded as follows. First, on the hardware level, the two dSPACE DS1104 control boards were replaced with an OPAL-RT OP5600-based control system. The new system provides 16 16-bit analog-to-digital (A/D) channels and 16 16-bit digital-to-analog (D/A) channels in a single chassis, as opposed to 8 16-bit and 8 12-bit A/D channels along with 16 16-bit D/A channels split over two unsynchronized boards in the older configuration. The new OP5600-based system is able to read three load-cells in each of the three axes and five LVDTs (two on horizontal axes and three on the vertical axis), in addition to a string-potentiometer (SP) to enable coarse displacement-based control of the vertical axis during test set up (Fig. 2.4). These sensors utilize nine A/D channels leaving seven A/D channels free for additional sensors (such as pore-pressure sensors) that may be added at a later date. Three D/A channels are utilized to drive the servo-valves associated with the hydraulic actuators for the

three axes, leaving 13 D/A channels for additional actuation functions. All channels are synchronized using the clock of a field-programmable gate array (FPGA).

With the OP5600, the computational power of the system has also been greatly enhanced where a 2.4 GHz 4-core CPU is used instead of the 250 MHz PowerPC 603e processor on the DS1104 boards. The OP5600 also has 2 GB of RAM instead of a total of 40 MB of on-board memory on the DS1104, allowing longer-data records or more channels to be captured at high sampling rates.

Displacement as well as load-based control of the vertical axis has been added as part of the device upgrade. Moreover, feedback control of the vertical axis allows consolidation to be performed using user-specified strain rates (within given tolerable error thresholds). The device has been equipped with a hydraulic power supply (MTS Model 506.02). The hydraulic pump provides a continuous operation pressure of 207 bars (20,700 kPa) and a flow rate of 22.8 l/m.

For the horizontal axes, the high-performance MIMO control algorithm (Duku et al. 2007) was replaced with decoupled PID control in each axis. The MIMO controller had been implemented to improve multiaxial tracking control by compensating for motion induced in one axis due to the motion in the other. For the present application, we have returned to a simpler PID-based control of the horizontal axes, as the additional changes in the control system for the vertical axis significantly complicate application of MIMO control algorithm in the horizontal direction to the point that it was deemed impractical.

2.4 SYSTEM PERFORMANCE

Duku et al. (2007) evaluated the performance of the DC-SS system, which includes the controller, pump, actuators and servo valves. Performance was quantified by the misfit between command and feedback horizontal signals for a variety of conditions, including sinusoidal and broadband loading applied along one or both of the horizontal axes. Some of the key results of that performance testing were:

- There is a baseline level of noise in horizontal feedback signals that is controlled by the A/D converter. The noise had a nearly flat Fourier amplitude spectrum suggesting white

noise characteristics; in the time domain the noise has zero mean and a standard deviation of approximately 0.0003 mm.

- Errors in command signal tracking were generally quite low, but increased as the amplitude of the command signal decreased and the frequency increased.
- Errors in command signal tracking for a reference (baseline) horizontal direction increase by approximately a factor of four when shaking is applied in the perpendicular horizontal direction.

In the sub-sections that follow, we re-evaluate these performance attributes using the newly configured control system. We also investigate the performance of the constant height control feature, and quantify top-cap rocking effects which has not been documented previously.

2.4.1 Horizontal axes performance

We begin by re-evaluating the horizontal axis performance originally investigated by Duku et al. (2007). This re-evaluation is motivated by the potential for changes in the performance due to the change to PID control, the use of a new pump, and the potential for degradation of the servo-valves over time.

Figure 2.5a compares the command (x_i^c) and feedback (x_i^f) signals in the time domain for a sinusoidal command signal with an amplitude of 0.01 mm in one direction having a frequency of 1 Hz; the feedback signal has been adjusted for a phase shift of 0.03 sec, which is consistently observed regardless of loading amplitude and frequency. The LVDT feedback signals were recorded using a sampling frequency of 1000 Hz. Index *i* refers to time step, and varies from one to *N*. Figure 2.5b shows the error term $x_i^f - x_i^c$ along with a typical feedback signal when the system is operational but the command is set to zero. The command and feedback signals are very well matched in amplitude at the control frequency of 1.0 Hz as well as at higher and lower frequencies.

The maximum mismatch between the command and feedback signals occurs at the times where maximum displacement occurs. The amplitude of $x_i^f - x_i^c$ is higher than the noise in the system with no command signal (Figure 2.5b). However, as shown by the Fourier spectra in Figure 2.5(c), the difference between these signals is dominated by low frequencies (i.e., the frequency of the command signal) and their amplitudes match beyond approximately 8 Hz. This

shows that system noise unrelated to the control system (i.e., from the pump or A/D converter) dominates the mismatch between command and feedback signals away from the control frequency. As shown in Figure 2.5c, the noise level is practically identical with and without the pump having been turned on, indicating that the pump is not significantly contributing to this error. The noise must, therefore, be associated with the A/D converter.

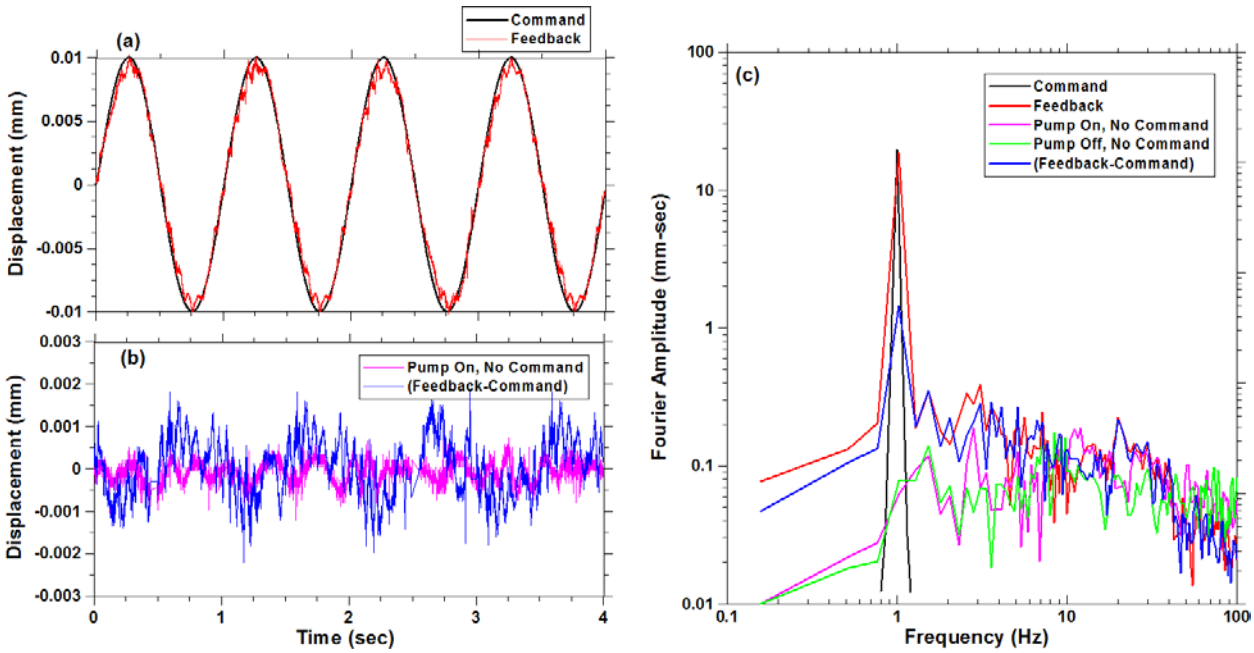

Figure 2.5. Sinusoid tracking of a cyclic displacement amplitude=0.01 mm for shearing along one axis at a time (a) command versus feedback signal, (b) evaluation of A/D performance, (c) FFT of the signals and noise

The normalized root mean square error (ε_{RMS}) of the feedback signal can be calculated as:

$$\varepsilon_{RMS} = \sqrt{\frac{\sum_{i=1}^{N}\left(x_i^f - x_i^c\right)^2}{\sum_{i=1}^{N}\left(x_i^c\right)^2}} \tag{2.1}$$

where the summation occurs over time. Values of ε_{RMS} for the excitation shown in Fig. 2.5a was computed to be 16%. Figure 2.6 presents the variation of ε_{RMS} with displacement amplitude and frequency in unidirectional tests, along with the prior results of Duku et al. (2007) for 1 Hz shaking. Error term ε_{RMS} increases with decreasing displacement amplitude and increasing frequency of excitation. The increase of error with decreasing amplitude results from the

increasing significance of system noise; the increase of error with frequency results from the increased significance of small phasing errors that are not compensated for by the phase shift of 0.03 sec that was applied to the feedback signal. The errors for the 1 Hz control frequency have increased somewhat from those recorded by Duku et al. (2007); The reason for the increased error is that we have reverted to a PID-based control system instead of a non-robust MIMO control system which provided better tracking performance for the relatively simple constant vertical loading, and was tuned for particular loading conditions. However, with 'robust' PID control (meaning that it can operate over a range of vertical loads), we are now able to catch lower strains, since we are taking advantage of differential analog-to-digital converters which reduce the noise in the LVDT signals.

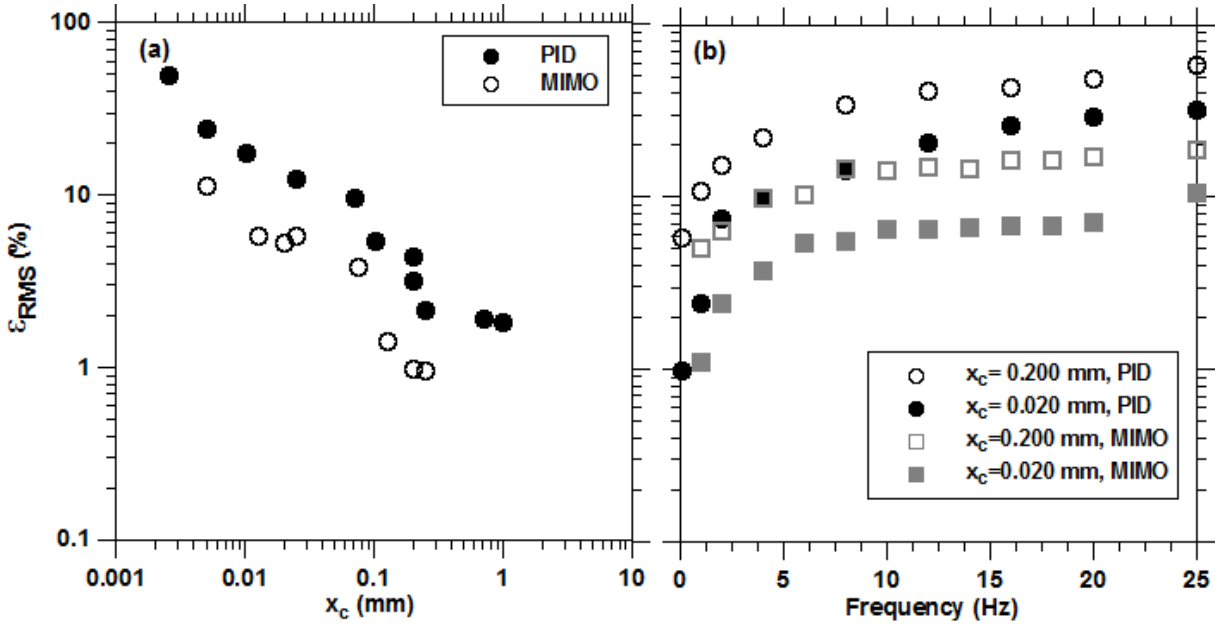

Figure 2.6. Variation of tracking error for unidirectional shaking with (a) displacement amplitude and (b) command frequency from present study using PID control and Duku et al. (2007) using MIMO control.

The effects of interaction between system responses in two horizontal directions were investigated by maintaining a consistent command signal along an arbitrarily chosen baseline axis (amplitude of 0.20 mm; 1 Hz frequency) while commanding the perpendicular horizontal axis with signals of identical amplitude but variable frequency (0 to 25 Hz). Figure 2.7 shows the resulting error terms per Eqn. (2.1) for the baseline axis feedback signals. As with Duku et al.

(2007), we see that error on the baseline axis is increased by excitation on the perpendicular axis, but that the error terms are not significantly frequency dependent beyond 2 Hz. In particular, there is no increase of error near the oil-column resonant frequency of the hydraulic cylinders, which is approximately 17 Hz (Duku et al., 2007).

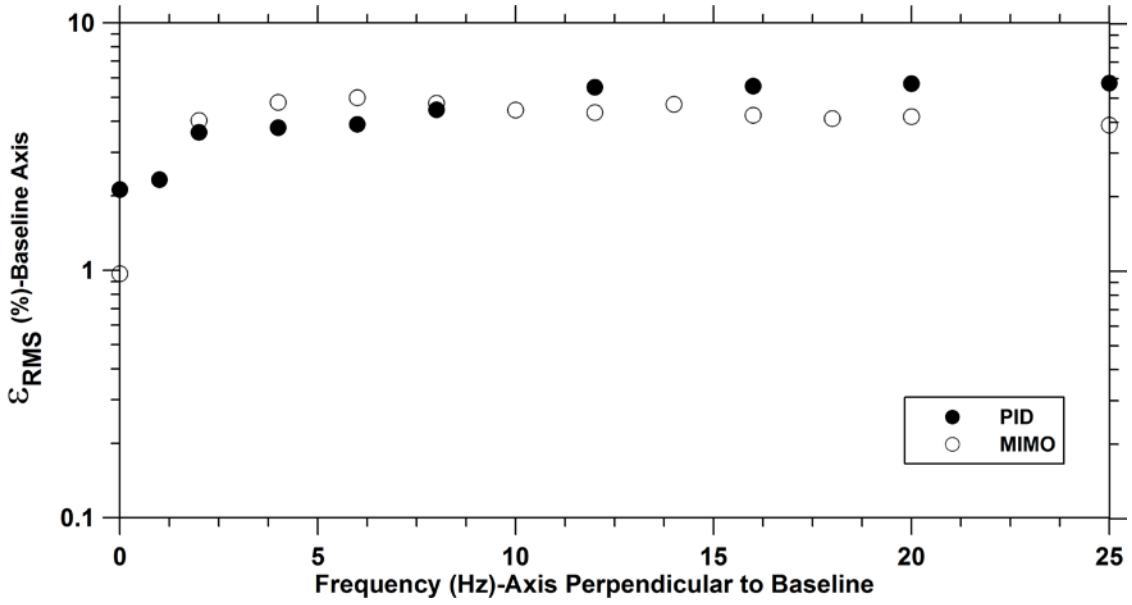

Figure 2.7. Normalized root mean square of tracking errors on baseline axis for varying frequencies of excitation on perpendicular axis under present configuration using PID control and Duku et al. (2007) using MIMO control.

The tracking error results presented previously (Figures 2.5 to 2.7) were obtained from tests carried out without amplifying the horizontal LVDT signals prior to A/D conversion. Since the A/D converter can be a significant source of noise, there is potential benefit to pre-digitization amplification to increase the signal-to-noise ratio. To investigate this effect, we re-evaluated the dependence of ε_{RMS} with displacement at 1.0 and 0.1 Hz command frequencies using a pre-digitization amplification (or "gain") of 10. As shown in Figure 2.8, the benefit of amplification is negligible for low frequencies and large command amplitudes, but to improve tracking by up to a factor of approximately three at 1.0 Hz excitation and the lowest amplitudes considered of 0.001 to 0.0025 mm. It is noteworthy that the shear strain associated with a displacement of 0.001 mm (assuming a specimen height of 2 cm) is 0.005%, which is well below the minimum strain considered previously by Duku et al. (2007) and Yee et al. (2011). This has significant

ramifications for the potential to measure small strain damping D_{min} and various threshold strain parameters with the DC-SS device (Vucetic et al. 1998, Mortezaie and Vucetic 2012).

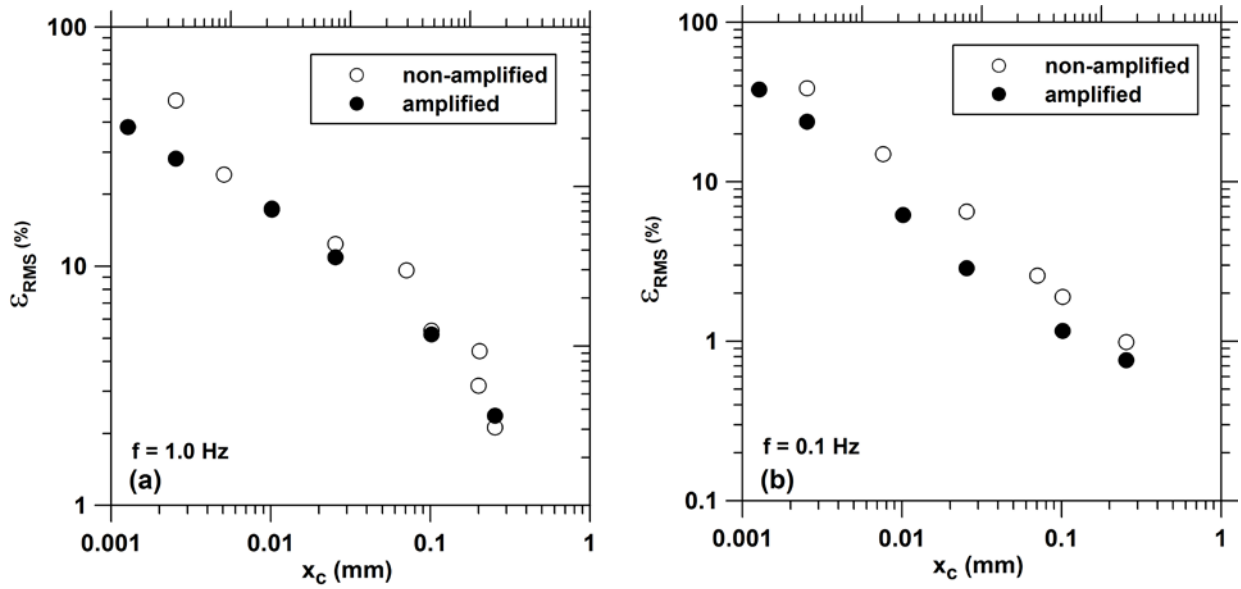

Figure 2.8. Effect of amplifying feedback signal prior to A/D conversion on the normalized root mean square error for harmonic excitation at (a)1.0 Hz and (b) 0.1 Hz

2.4.2 Vertical axis performance

The principal capability that has been introduced to the DC-SS device is functionality to maintain constant height conditions while varying the vertical stress through the control algorithm. Figure 2.9 presents the results of a strain-controlled test on dry sand at 52% relative density under constant height conditions. The strain history is seen to be maintained at a steady amplitude, but the shear and normal stresses decrease with the number of cycles. The decrease of normal stress with number of cycles is interpreted as an equivalent pore pressure, as described in Section 2.3.1. Figure 2.9d shows the variation with time of vertical strain, which reaches values as high as 0.027% but should ideally be zero if the control algorithm were working perfectly. In this subsection, we formally quantify the error in vertical top cap displacement from the feedback system (z_i^f) relative to the command level of $z_i^c = 0$ for i=1:N.

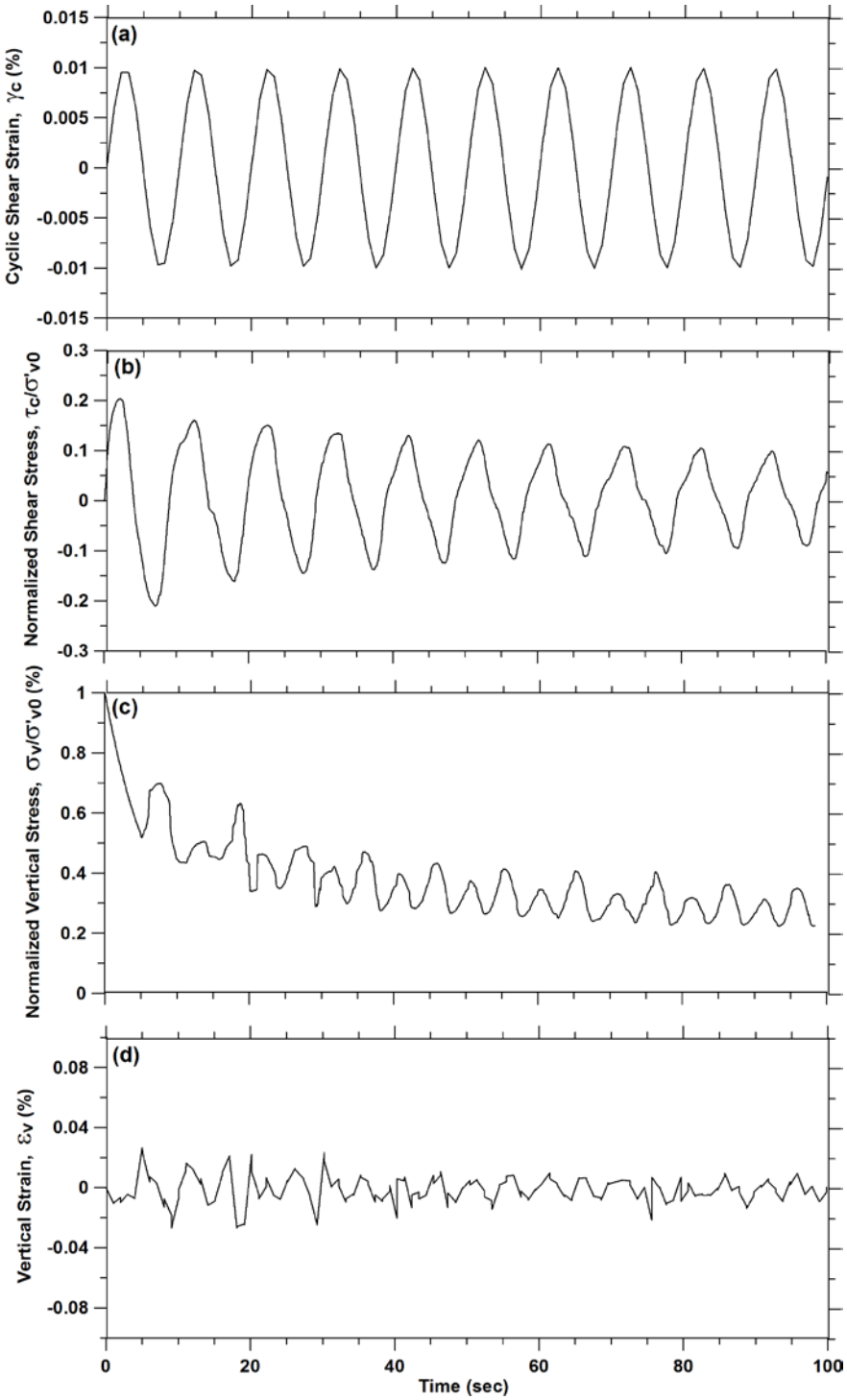

Figure 2.9. Constant height strain-controlled test on Silica No.2 dry sand under an initial vertical stress (σ'_{v0}) of 100 kPa, and a frequency of 0.1 Hz.

We quantify error in a similar manner to that for the horizontal axes using a root mean square differential between feedback and command. However, unlike Eq. (2.1), we cannot normalize by the sum of the square of the command signal, because that is zero, making the normalized error undefined. Instead, we normalize by the product of number of data points N and initial height h_0, which makes our error term akin to a standard deviation of vertical strain.

$$\varepsilon_{VRMS} = \frac{1}{h_0}\sqrt{\frac{\sum_{i=1}^{N}(Z_i^f - Z_i^c)^2}{N}} \tag{2.2}$$

Figure 2.10 shows the performance of the constant height vertical axis control algorithm in terms of ε_{VRMS} plotted against the horizontal displacement amplitude for excitation frequencies of 1.0 and 0.1 Hz. Excitation is in one horizontal direction. We find ε_{VRMS} to increase with horizontal displacement amplitude and to be essentially frequency-independent. Even at the largest displacement considered of 1 mm (corresponding approximately to 5% shear strain), the vertical strain error is less than 0.04% which is much less than ε_{RMS} (Fig. 2.6a).

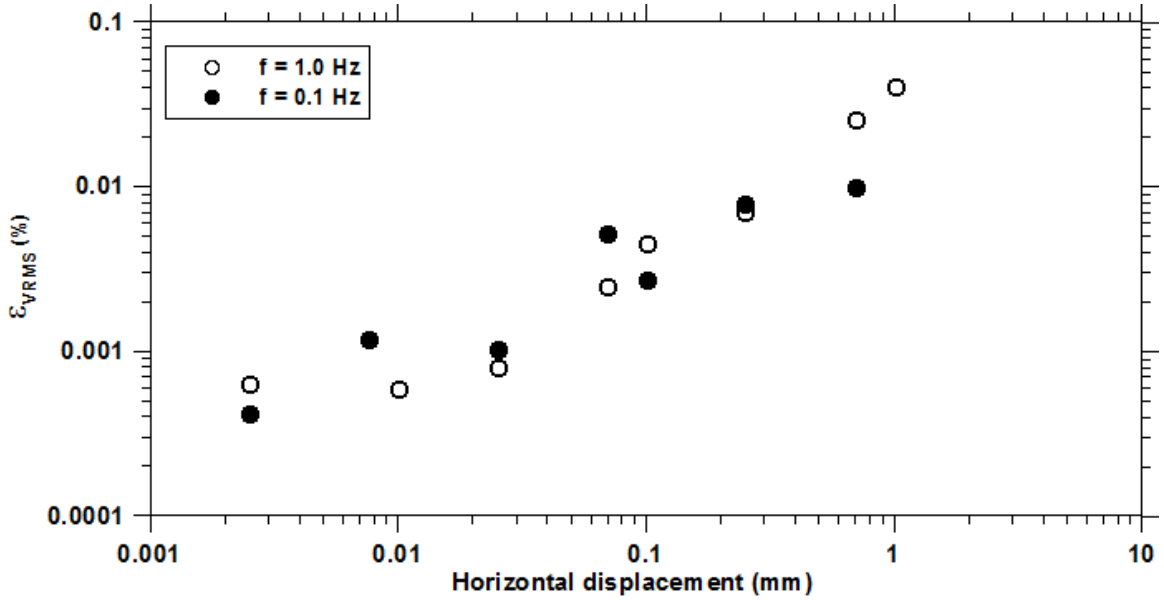

Figure 2.10. Performance of vertical axis in maintaining constant height condition

Prior investigations of vertical control error have been undertaken by Degroot et al. (1991) and Porcino et al. (2006). Degroot et al. (1991) tested a normally consolidated clay under monotonic loading and enforced constant height conditions using a control system interfacing with a servo-pneumatic actuator. Using a single LVDT on the top cap, they observed a maximum vertical strain of 0.003%. Porcino et al. (2006) similarly sheared dry sands monotonically, enforcing constant height conditions using a control algorithm with an electro-mechanical actuator. They reported a maximum vertical strain of 0.015%, again from a single LVDT. Recall that the UCLA DC-SS device uses three LVDTs on the top cap.

The use of a single LVDT on the top cap is potentially problematic if there is top cap rotation, which is difficult to eliminate. In the presence of such rotation, the LVDT is likely to capture the sum of the average vertical displacement and the vertical displacement from top cap rotation at the LVDT location. Our view is the average vertical displacement, which effectively removes rotation effects, provides a better basis for control than does a point measurement from a single LVDT. While we cannot know the extent to which rocking affected the vertical control achieved by Degroot et al. (1991) and Porcino et al. (2006), it is nonetheless encouraging that the levels of control achieved in our tests compare favorably, especially given the relatively rapid loading rates and cyclic conditions imposed in the present test program.

2.4.3 Rocking

A common problem in simple shear testing is rocking of one end cap relative to another during shear, which leads to undesirable stress concentrations around the specimen perimeter. Our search reveals that the amount of rocking in terms of rotation/vertical deformation has not been well documented in past studies of simple shear device performance. Rutherford (2012) recently measured the torques resulted from rocking in a direct simple shear device by using multi-axis load cell. Hence, that study adopted a ‘force-based’ representation of the rocking effects, which does not measure actual rocking. We take a different approach, which is to directly measure rocking of the specimen top cap using measurements from multiple LVDTs.

As described by Duku et al. (2007), the DC-SS device was designed with a tri-post frame and high performance track bearing to accommodate vertical displacement of the top cap and

minimize cap rocking (Figure 2.3b). The recent device upgrades include a rigid connector between the top cap and actuator to further restrain rocking.

Figure 2.11a shows the top cap rocking for a cyclic strain-controlled, constant volume test on a dry sand under an initial over burden pressure (σ_{v0}) of 100 kPa. The cyclic loading was applied with a shear strain amplitude (γ_c) of 4% and a frequency of 1 Hz. Assuming excitation in the *x* direction, angular distortion θ_{yy} indicates rotation within the vertical plane parallel to the *x*-axis, whereas θ_{xx} indicates rotation in the vertical plane perpendicular to the direction of excitation. These rotations are defined from the three LVDTs mounted on the specimen top cap. Figure 2.11a shows the expected result that $\theta_{yy} > \theta_{xx}$ for excitation in the *x*-direction. Note that the amount of rocking decreases with the amplitude of the shear and vertical loads. Vertical deformations from top cap rocking can be expressed in a normalized form as follows:

$$\varepsilon_{\theta RMS} = \frac{1}{h_0}\sqrt{\frac{\sum_{i=1}^{N}\left(R\theta_{yy,i}\right)^2}{N}} \tag{2.3}$$

where *R* is the specimen radius. A similar error term can be defined using θ_{xx}. Figure 2.11b shows the performance of the device in restraining the rocking in terms of $\varepsilon_{\theta RMS}$ resulted from angular distortion, θ_{yy} plotted against the horizontal displacement amplitude for excitation frequencies of 1.0 and 0.1 Hz. Excitation is in one horizontal direction. The value of $\varepsilon_{\theta RMS}$ resulted from θ_{xx} is not shown in Figure 2.11b, since its related vertical displacements are negligible ($< 3\times10^{-4}\%$), falling in the range of precision of the LVDTs. We find $\varepsilon_{\theta RMS}$ to increase with horizontal displacement amplitude and to be essentially frequency-independent. Even at the largest displacement considered of 1 mm (corresponding approximately to 5% shear strain), the vertical strain error is less than 0.02%. The value of $\varepsilon_{\theta RMS}$ is approximately half of ε_{VRMS} (Figure 2.10).

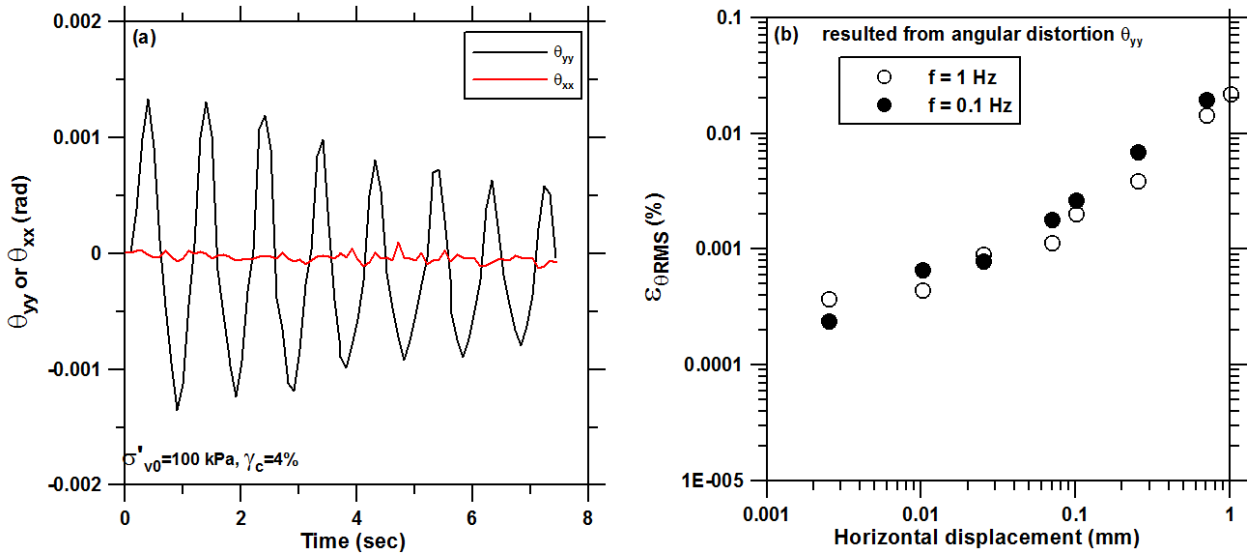

Figure 2.11. Performance of the UCLA DC-SS device in restraining rocking (1) angular distortions in a cyclic strain-controlled test (2) error term related to the vertical deformation caused by rocking

2.5 CALIBRATION TESTS

To demonstrate the capabilities of the device, specimens of dry sands and nearly saturated clay were subjected to monotonic and cyclic loading under drained and undrained conditions. The soil behavior for these materials and test conditions are well understood from information in the literature so that the results from the present device configuration can be compared. Cyclic strain-controlled drained tests were first performed to ensure that the new control system yields similar volume change results to those obtained by Duku et al. (2008). Then, constant volume tests were performed to verify if the device can capture typical behavior of sand and clay specimens under undrained conditions. All the tests presented here were performed on specimens with a height and diameter of 25.4 and 72.6 mm, respectively.

2.5.1 Seismic Compression of Silica No.2 Dry Sand

Duku et al. (2008) used the UCLA DC-SS device to investigate seismic compression of dry clean sands. One of the materials considered in their study was Silica No. 2 with D_{50} =1.60 mm and maximum and minimum dry densities of 1.610 and 1.349 gr/cm^3, respectively. As the first step in evaluating the capabilities of the new control system, cyclic strain-controlled drained tests were carried out on Silica No. 2 dry sand at relative densities of 45 and 80% for comparison to

the prior results of Duku et al. (2008). The dry pluviation method was used to form the specimens. As needed, the bottom cap was tapped with a plastic hammer to densify specimens.

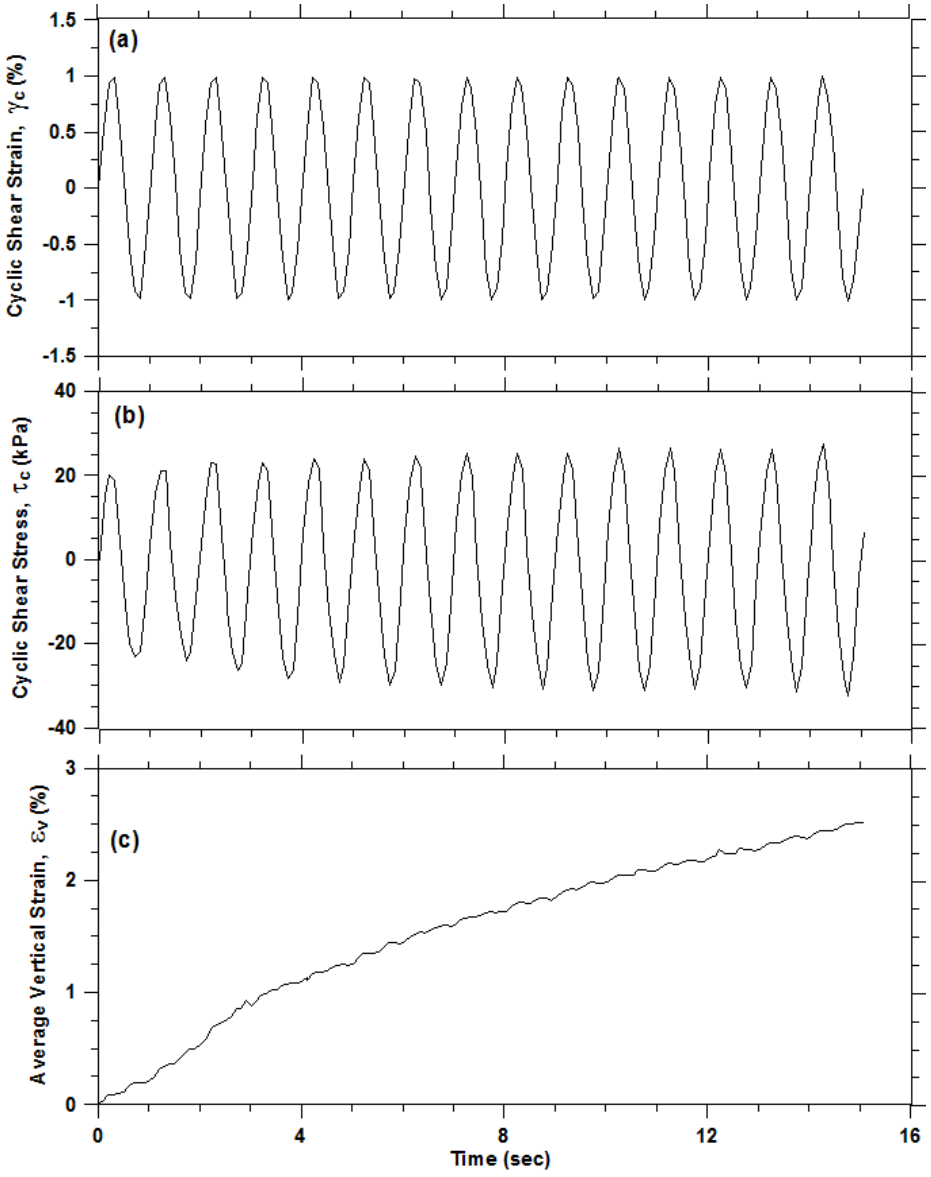

Figure 2.12. Cyclic strain-controlled simple shear test results on a dry sand (Silica No.2, D_r=45%)

All the tests were performed at a frequency of 1 Hz, and continued up to 15 cycles. Figure 2.12 shows the results of a strain-controlled test on Silica No. 2 when shear strain amplitude (γ_c) is 1.0%, and relative density (D_r) is 45%. The data show that cyclic shear stress (τ_c) slightly increase during the first few cycles until the soil's equivalent shear modulus stabilizes (Figure

2.12b). The rate of accumulation of vertical strain (ε_v) decreases with time (Figure 2.12c). These are typical patterns of behavior observed in many previous tests.

Tests similar to that illustrated in Figure 2.12 were repeated for many strain levels and the aforementioned relative densities of 45% and 80%. Figure 2.13 compares the seismic compression after 15 cycles ($\varepsilon_{v,N=15}$) from the present testing (with the new control system) with prior results from Duku et al. (2008) on similar Silica No. 2 sand specimens. The mean model prediction in Figure 2.13 was plotted taking into account the material term η_i, which is 0.12 for Silica No. 2 sand (i.e., this is the mean misfit of the data at about 1% shear strain relative to the Duku et al. model; details in Yee et al. 2013). The current results are seen to be near the mean of the material-specific relationship.

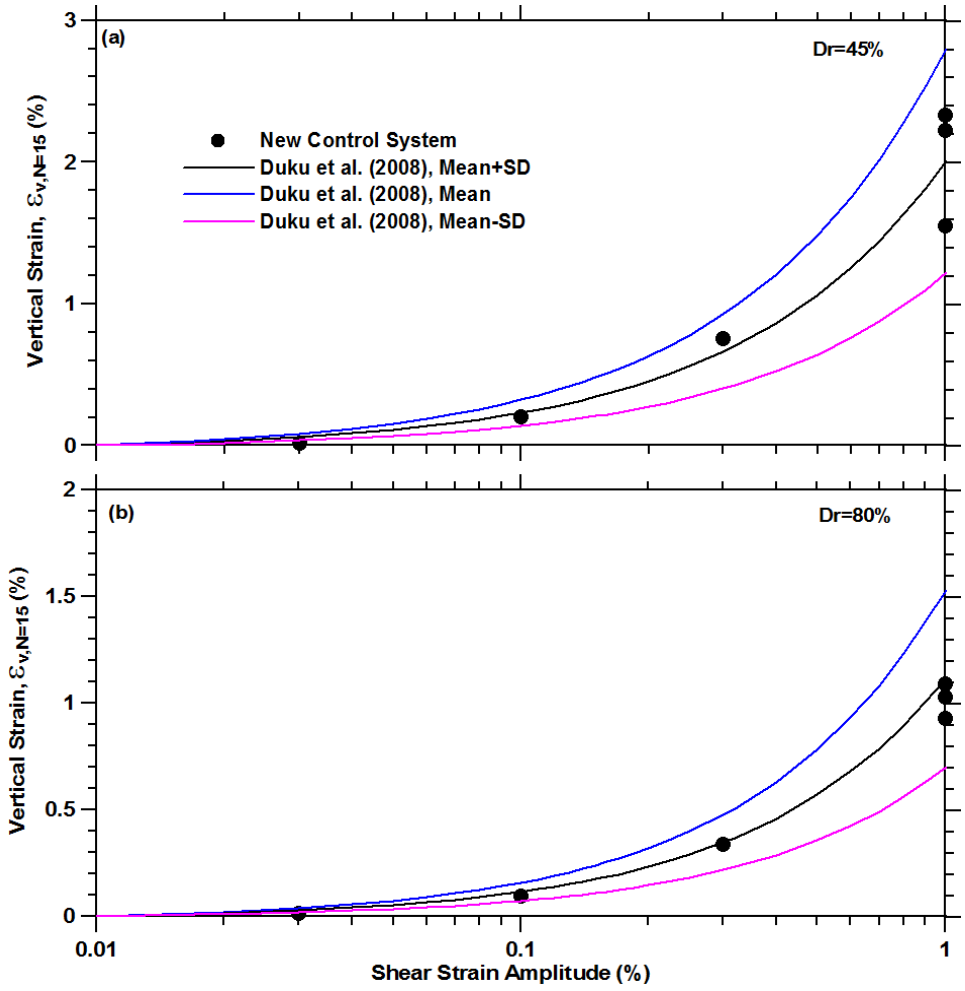

Figure 2.13 Performance of the new control system in terms of seismic compression of Silica No. 2 sand

2.5.2 Cyclic behavior of Silica No. 2 dry sand under constant-height conditions

To investigate the constant height capabilities of the DC-SS device, cyclic strain-controlled tests were performed on Silica No. 2 dry sand at two different densities: D_r=30%, and D_r=52%. The tests were performed under an initial vertical stress of σ_{v0}'=100 kPa, a shear strain amplitude of 1%, and a frequency of 0.1 Hz. The change in vertical stress is taken as the change in pore water pressure. As shown in Figures 2.14a and b, the relatively loose sand shows significant degradation and pore water pressure ratio (r_u) reaches close to 1 after 10 cycles which is an indication of liquefaction. On the other hand, as shown in Figs. 2.14c and d, the medium dense sand exhibits less degradation and higher shear moduli (i.e., the slope of hysteresis loops) with respect to the loose sand. Pore water pressure is stabilized around $r_u = 0.7$ for large numbers of cycles. These are strain controlled tests and thus do not indicate clear dilatency as observed in liquefied specimens of sand subjected to stress-controlled tests.

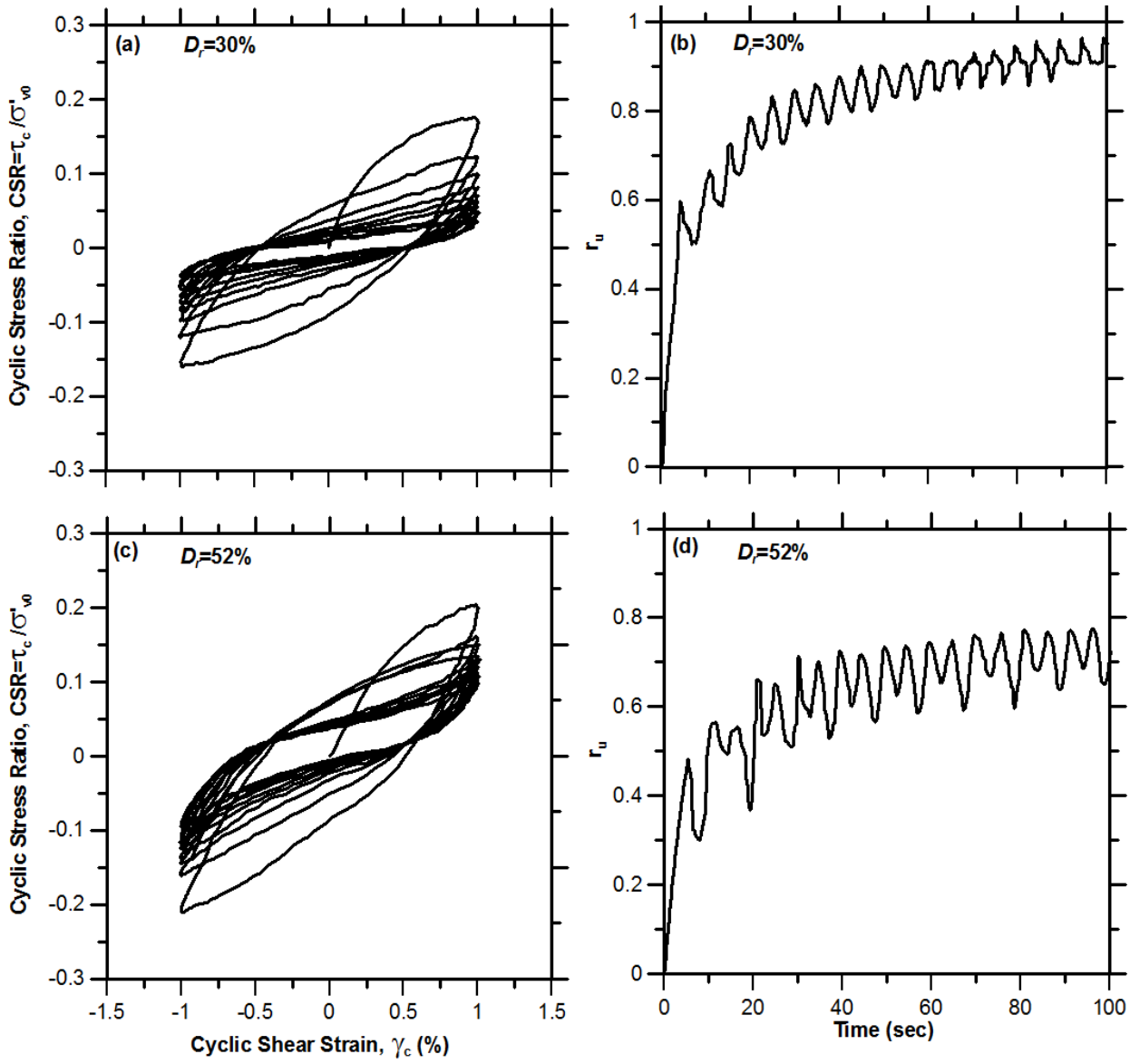

Figure 2.14. Cyclic behavior of Silica No.2 dry sand under constant volume conditions at different densities

2.5.3 Monotonic behavior of Flint No. 16 dry sand under constant-height conditions

We further investigate the constant height capabilities of the new control system by examining the monotonic shear behavior of loose Flint No. 16 dry sand. In these tests we seek to examine phase transformation behavior of soils that are contractive at small strains and then become dilatant at large strains. Flint No. 16 is a fine sand with D_{50}=0.50 mm, and maximum and

minimum dry density of 1.778 and 1.493 gr/cm^3 respectively. The dry pluviation method was used to prepare loose specimens of Flint No. 16 sand with a relative density of 18%. The tests were performed at three different initial vertical pressures (σ_{v0}) of 50, 100 and 200 kPa.

Figures 2.15a and b present the shear stress-shear strain and stress path (i.e., vertical effective stress versus shear stress) response of the tested material. As shown in Fig. 2.15b, at the beginning of the loading significant pore water pressure generates, irrespective of initial vertical pressure. Once the stress path touches the phase transformation line, negative pore water pressure generates and soil behavior becomes dilatent as indicated by rapidly increasing shear stress. Similar trends were reported by Ishihara (1993) from testing on loose specimens of Toyoura sand with D_r =16% under triaxial compression stress paths.

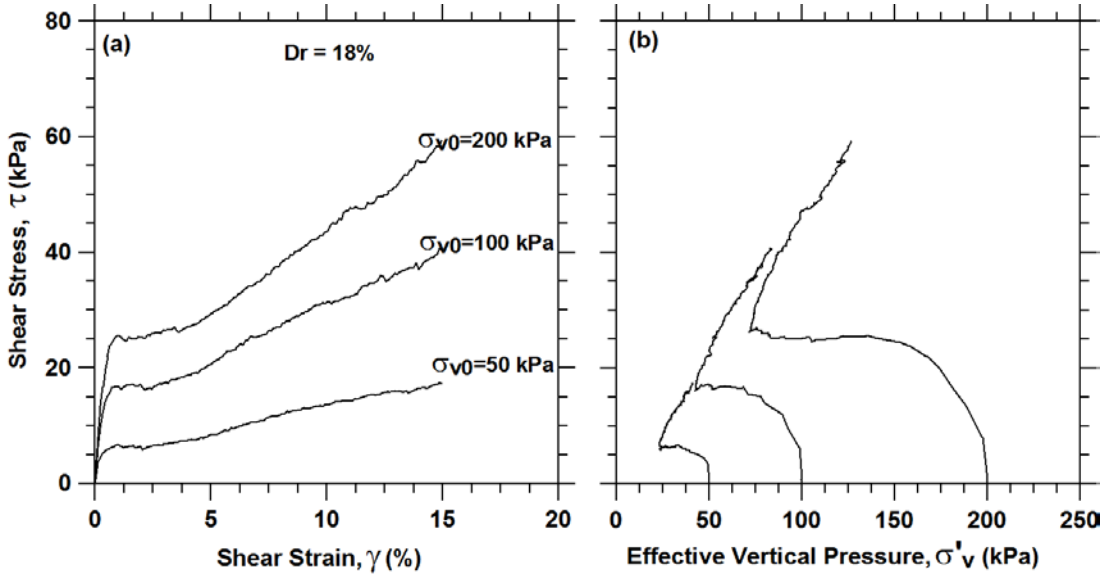

Figure 2.15. Monotonic behavior of Flint No.16 dry sand under constant volume conditions at D_r=18%

2.5.4 Monotonic behavior of a normally consolidated clay under constant-height conditions

It is well known that saturated clays show normalized behavior when tested monotonically under undrained conditions. For instance, Ladd (1991) showed that normalized undrained shear strength (S_u/σ'_{v0}) in normally consolidated clays under triaxial compression is almost constant (S_u is undraind shear strength, and σ'_{v0} is the initial vertical effective stress). He also showed that S_u/σ'_{v0} under simple shear condition is less than that of triaxial compression, and is weakly dependent on the plasticity index (PI) of the tested material.

To make sure that the UCLA DC-SS device can capture normalized behavior of clays, monotonic undrained tests were performed on a low plastic normally consolidated clay with PI=12. Reconstituted samples were prepared by first pouring the clay slurry into a Shelby tube. Next, the slurry was loaded vertically by a piston that exerts a small vertical pressure as low as 10 kPa. Following primary consolidation, the sample was carefully extracted, trimmed and placed in the simple shear device. It was subsequently consolidated to a higher consolidation stress in the simple shear device to limit the effects of sample disturbance. The tests were performed at three different initial vertical pressures (σ_{v0}) of 50, 100 and 200 kPa. The normalized shear stress-strain and stress paths shown in Fig. 2.16 are similar to the typical behavior of normally consolidated clays (e.g., Atkinson and Bransby 1978), and provide a normalized shear strength (S_u/σ'_{v0}) for all three materials that is about 0.20. Ladd (1991) showed that S_u/σ'_{v0} of normally consolidated clays with PI around 12 under simple shear loading condition falls between 0.19 to 0.26. Hence, the observed behavior exhibits normalization and typical levels of shear strength.

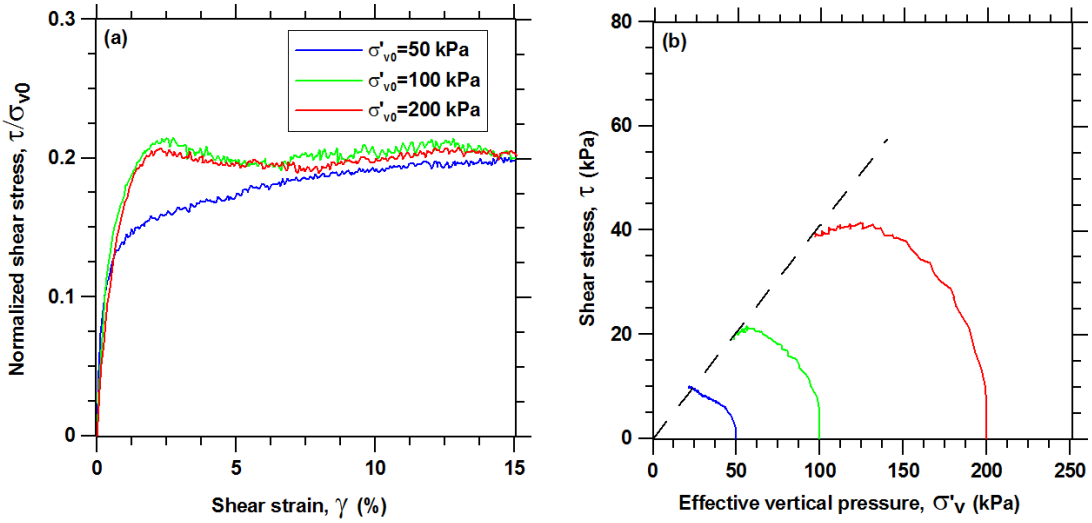

Figure 2.16. Monotonic behavior of a low plastic normally consolidated clay under constant volume conditions

3 Mechanical Behavior of Sherman Island Peat

3.1 INTRODUCTION

Peat is a mixture of fragmented organic materials formed in wetlands under appropriate climatic and topographic conditions and it is derived from vegetation that has been chemically changed and fossilized (Edil and Dhowian, 1981). Peat-producing ecosystems are found throughout the world, and peat deposits constitute 5 to 8% of the land surface of the earth (Davis 1997).

Peat is often considered a problematic soil due to its low shear strength, high compressibility, water content, and organic content. Its color is usually dark brown, grey or black and with a distinctive odor. Since the main component is organic matter, peat is very spongy, and combustible.

Previous geotechnical studies of peaty organic soils can be categorized into three general themes: (1) laboratory characterization of the compressibility of peat under static loading conditions; (2) laboratory characterization of the shear modulus and damping characteristics of peat, which is applicable to analysis of earthquake ground motions propagating through peat but not to the analysis of ground failure; (3) laboratory characterization of dynamic pore pressure generation and its associated effects of strength loss and post-cyclic volume change.

A number of researchers have characterized the shear modulus and damping ratio of peat as a function of cyclic shear strain. As described by Wehling et al. (2003), tests performed on peats from Mercer Slough in Washington (Kramer, 2000), Queensboro bridge in New York (Stokoe et al., 1996), and Sherman Island in California (Boulanger et al., 1998; Wehling et al., 2003) show a wide range of behavior from relatively linear (i.e., modest modulus reduction, modest damping) at high effective consolidation stresses (near 100 kPa) to strongly nonlinear at low stresses (generally 10-40 kPa). Testing performed on relatively undisturbed tube samples along with pre-sheared and re-consolidated specimens indicated that the effect of sample disturbance on the modulus reduction and damping relations was small (Wehling et al., 2003). Kishida et al.

(2009) developed regression models for the dynamic properties of highly organic soils. They showed that shear modulus and damping ratio are a function of shear strain amplitude, consolidation stress, and organic content.

In this chapter, we describe a testing program undertaken to fill a gap in the literature concerning Item (3) above on cyclic pore pressure generation and its effects on strength loss and post-cyclic volume change. We describe the test site, sampling procedure, the tested material, sample preparation, and test results. As part of the data interpretation, we introduce new concepts on the 'resetting' of secondary compression as a result of loading that generates pore pressure and the effects of cyclic pore pressure generation on post-cyclic volume change.

3.2 SITE CHARACTERISTICS AND SAMPLING TECHNIQUE

Nine boreholes were drilled, and 24 undisturbed 0.45m long samples were taken from a free-field site on Sherman Island at different depths ranging from approximately 1 to 6 m. This site was used for cyclic testing of a model levee using a mobile eccentric mass shaker (Reinert et al., 2013). Soil samples were obtained with a piston sampler designed to be deployed in a hand auger borehole. We found that the unsupported borehole would squeeze shut at a depth of typically 2 to 3 m, so the piston sampler was lowered to the bottom of the borehole and subsequently advanced by hand to the desired depth with the piston locked at the bottom of the tube. This procedure can only be utilized in extremely soft soils weak enough to permit the sampler to be pushed by hand through the soil. When the sampler had been advanced to the desired depth, the piston was unlocked and the tube was pushed into the peat. Water was poured on top of the piston to generate suction to help retain the sample, and the sampler was subsequently retracted. We obtained full recovery for every sample once this procedure had been applied.

Figure 3.1 illustrates the geotechnical conditions at the test site, including cone tip resistance, shear wave velocity, and interpreted stratigraphy. Shear wave velocity was measured at the site using surface wave methods (i.e., spectral analysis of surface waves, SASW). The dispersion curve was not inverted to obtain a shear wave velocity profile, but an average shear wave velocity of only about 25m/s was inferred. For comparison, a suspension logging profile from the nearby Antioch bridge site is included (GeoVision 2000), and provides reasonable agreement with the SASW measurement. The top 11 m of the site consists of peaty organic soils, which are locally compressed beneath levees (Wehling et al. 2003). Formation of this peaty organic soil

stratum began about 11,000 years ago from decomposition of plant materials (CDWR 1992). The peat stratum is underlain by sand-silt dune deposits, which extend to the maximum depth locally explored of 20 m. As shown in Fig. 3.1, the peat layer has very low (near zero) CPT tip resistance (q_c) and a mean V_s of approximately 22 m/s. A simple surface wave travel time measurement at the site confirmed that the average Rayleigh wave velocity in the peat was about 26 m/s, as shown in Fig. 3.1.

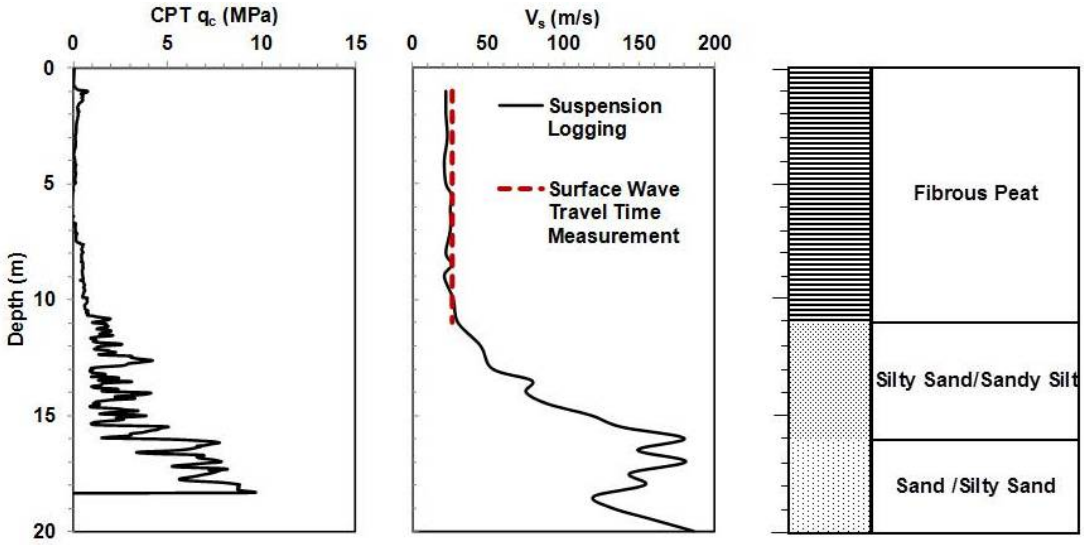

Figure 3.1. CPT tip resistance (q_c), and shear wave velocity (V_s) from a free-field site on Sherman Island (V_s profile from GeoVision 2000)

3.3 TESTED MATERIAL AND PROCEDURE

The samples used for testing of various types are summarized in Table 3.1. For this study, we focus on testing performed on samples from a depth range of 1.3-3.0 m, which is below the seasonally fluctuating water table. Index tests indicate water contents ranging from 410% to 700% and specific gravity of 1.85. Consolidation tests on undisturbed samples were performed in a traditional consolidation cell based on the ASTM D2435 (ASTM, 2010) procedure, while the consolidation tests on the reconstituted specimens were performed using new procedures, described below, that do not conform with ASTM D2435 (ASTM, 2010).

Cyclic testing [direct simple shear (DSS) and cyclic triaxial (CTX)] was performed in several stages. In the first stage, the peaty organic soils were consolidated to the stresses indicated in Table 3.1, which are either the in situ free-field effective stresses at the sample depth (σ'_{vc}) or the

estimated consolidation stress beneath the crest of Sherman Island levees. These consolidation stresses correspond to anisotropic (K_0-consolidated) conditions for the DSS tests and isotropic conditions for the CTX tests.

Table 3.1 Testing plan for undisturbed and bulk samples taken from a depth of 1.3-3.0 m

Specimen	Borehole	Organic content (%)	Test	σ_c'* (kPa)	Time allowed for post-cyclic volume change measurement
3-1a	3	70	1 D-Consolidation	13 to 195	
8-1a	8	63	1 D-Consolidation	13 to 195	
8-3b	8	58	1 D-Consolidation	13 to 195	
8-4a	9	55	1 D-Consolidation	13 to 195	
9-3b	8	53	1 D-Consolidation	13 to 195	
9-4a	8	52	1 D-Consolidation	13 to 195	
8-3c	8	58	Cyclic CTX (after 1 week consolidation)	8	40 min
8-3d	8	58	Cyclic CTX (after 1 week consolidation)	40	40 min
9-3a	9	53	CTX	9	24 hrs
9-3a	9	53	CTX	18	40 min
9-3a	9	53	CTX	42	40 min
Reconstituted	Bulk	51	1 D-Consolidation	9 to 298	
Reconstituted	Bulk	51	1 D-Consolidation Resetting Test	9 to 75	
Reconstituted	Bulk	51	1 D-Consolidation Resetting Test	19 to 74	
Reconstituted	Bulk	51	CTX	15	40 min
Reconstituted	Bulk	51	DSS	15	22 min
Reconstituted	Bulk	51	DSS	42	22 min

*Isotropic consolidation stress for CTX, vertical consolidation stress for DSS and consolidation tests.

Following consolidation, strain- controlled multi-stage cyclic shearing was performed in stages having shear strain amplitudes ranging from 0.01 to 10% for the DSS tests and axial strains of 1.3×10^{-3} to 2.4% in the CTX tests (equivalent shear strains of 1.9×10^{-3} to 3.6%). Each stage of loading consisted of 15 uniform strain cycles at a loading frequency of 0.1 Hz. Undrained conditions were maintained during shearing for the CTX tests by closing the drain taps to the specimen, and for DSS tests by maintaining constant height conditions by servo-

hydraulic control of the vertical piston. Following each stage of cyclic shearing, the specimen was allowed to reconsolidate to its initial consolidation stress and volume changes were monitored. In DSS tests, this step simply involved restoring the original vertical stress, whereas in the CTX tests this involved opening drainage valves. Strain-controlled tests were preferred over stress controlled tests to be able to relate post-cyclic volume change values to the cyclic shear strain amplitude.

3.4 STATIC COMPRESSIBILITY OF PEAT

There are two principal sources of compressibility in soil (including peat) under static loads. When sustained static loading is applied, water pressures initially develop due to inadequate time for pore fluids to drain (referred to as an *undrained* condition), which subsequently dissipate slowly over time. The volume change associated with dissipation of this excess pore pressure as water flows out of the soil is referred to as *primary consolidation*, or just *consolidation*. A second form of volume change, referred to as *secondary compression*, occurs in combination with consolidation but is unrelated to pore pressure dissipation. As such, secondary compression continues after pore pressures have dissipated and consolidation is complete. The secondary compression of peat is caused by a number of factors, including biodegradation of the organic matter (Mesri and Ajlouni 2007), loss of water from inside plant cells at higher pressure, and possibly from rearrangement of inorganic clay minerals due to surface charge effects. Secondary compression is generally observed to occur at a rate that decays logarithmically with time, however, secondary compression can be reset when a significant change in pressure occurs. These changes in pressure are typically imposed in a laboratory consolidation device in which the load can be carefully controlled in stages. The dominant factors controlling the compressibility characteristics of peat include the fiber content, natural water content, void ratio, initial permeability, nature and arrangement of soil particles, and inter-particle chemical bonding in some of the soils (Mesri and Ajlouni, 2007).

The compression behavior of peat varies from the compression behavior of other types of soils in two ways: 1) the compression of peat is much larger than that of other soils, and 2) the creep portion of settlement typically plays a more significant role in determining the total settlement of peat than of other soil types. The primary consolidation of fibrous peat takes place very rapidly because the hydraulic conductivity of peat tends to be much larger than inorganic

fine-grained mineral deposits. Secondary compression can be large enough to obscure the transition from primary consolidation to secondary compression that is apparent in dial gauge readings versus time for inorganic mineral soils. An acceleration in secondary compression, termed tertiary compression by Fox and Edil (1992), has also been observed.

Figures 3.2a and 3.2b show settlement vs. time for a typical virgin compression increment from the consolidation tests using logarithmic and square root of time axes. The results in Fig. 3.2a illustrate the difficulty in identifying the time of end of primary consolidation (t_p), which is usually apparent as a distinct flattening of the slope in the log-time plot. The loading stage in Fig. 3.2 was held for 24 hours, which is far more than enough time for primary consolidation to have ended, therefore the settlement is dominated by secondary compression. The difficulty in observing the end or primary consolidation was also observed by Fox and Edil (1992). On the other hand, plotting the data versus the square root of time permits interpretation of the end of primary consolidation using Taylor's (1948) method. However, as described later, a better approach is to make pore pressure measurements during the consolidation test to directly observe the end of primary consolidation.

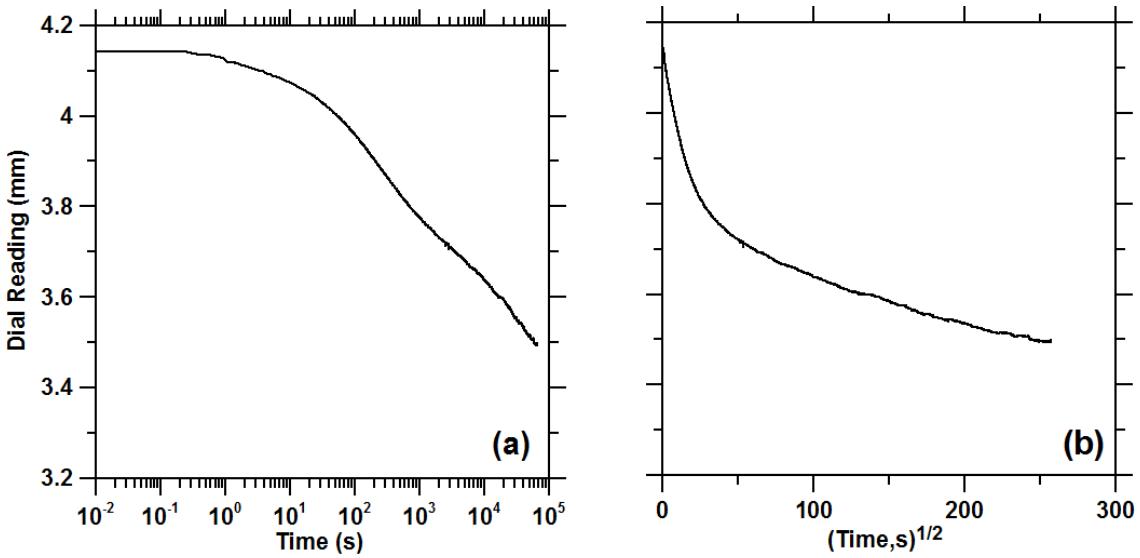

Figure 3.2. Typical settlement-time plots for an increment of load applied to peat. Specimen 8-3b, final σ'_{vc} =195 kPa

A consolidation curve in which the end of primary consolidation was evaluated using Taylor's method is shown in Fig. 3.3a. The stepped line indicates the volume change in each load increment from secondary compression (vertical steps) and primary consolidation (pair of sloped lines for recompression and virgin compression). The ensemble of points at the ends of load

increments falls below the consolidation curve due to secondary compression. The virgin compression index is interpreted from the consolidation curve as C_c=3.7, whereas the recompression index is C_r=0.2 based on the low-stress part of the unloading path. For the material tested in this study, C_c varies from 0.8 to 6.8, while C_r changes from 0.05 to 0.8 depending on the organic content (Fig. 3.3b). Mesri and Ajlouni (2007) indicated that fibrous peats display extreme compressibility, with compression index values 5 to 20 times the corresponding compressibility of typical soft clay and silt deposits.

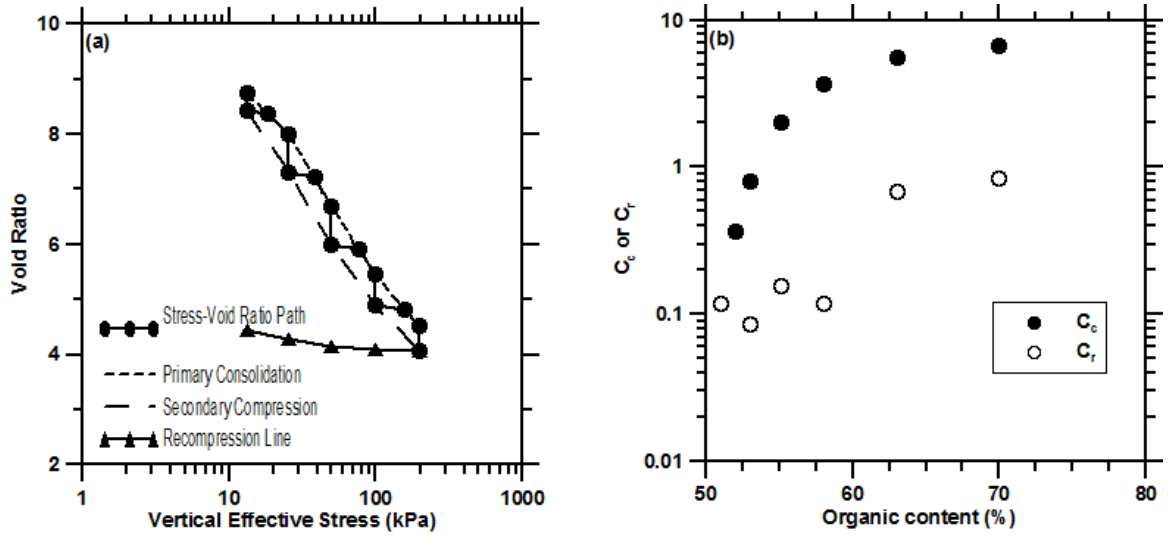

Figure 3.3. Consolidation behavior of the tested peat (a) loading-reloading sequences for the specimen 8-3b (b) Variation of C_c and C_r with organic content for the Sherman Island Peat

Using the portion of the settlement-time plots following t_p, the slope is computed from the change of void ratio over one log cycle of time (C_α). The ratio C_α / C_c was found to range from 0.044 to 0.065, following large virgin compression increments (i.e., increments in which the consolidation stress was doubled), with an average of 0.05. When the soil is overconsolidated (i.e., during unloading stages), C_α / C_c reduces to about 0.01 based on the traditional laboratory method for interpreting secondary compression (we will later demonstrate a clock resetting concept that may explain the slower secondary compression rate for overconsolidated soil).

3.5 COEFFICIENT OF SECONDARY COMPRESSION

The traditional method for estimating the coefficient of secondary compression from laboratory data involves the following steps: (1) apply a known load increment, typically an increment that

doubles the current vertical effective stress, (2) at the instant that the load is applied, start the clock on consolidation, (3) interpret the time at the end of primary consolidation, t_p, based on the dial gauge reading versus log-time plot, and (4) compute C_α based on the slope of the void ratio versus log-time plot for the straight line portion of the curve after t_p. This procedure suffers two problems when considering the potential for post-cyclic volume change in peat soils. First, secondary compression for peat is so large that there is often no break in the plot of dial gauge reading versus time (Fig. 3.2a), therefore t_p cannot be readily determined from a dial gauge reading alone. Second, reconsolidation after cyclic shearing is due to development of excess pore pressure, and the pore pressures generated in peat tend to be relatively small. Therefore the load increment imposed on the peat during recompression is much less than double the current effective stress. Each of these problems is addressed in detail in the following sections.

3.5.1 Development of new consolidometer to permit pore pressure measurement for determining t_p

To facilitate accurate determination of the end of primary consolidation, we designed and fabricated a new consolidometer that provides single drainage through the top of the specimen, while pore pressure is measured through the bottom of the specimen (Fig. 3.4). A similar device was utilized for peat by Fox and Edil (1999). This is different from a traditional consolidation device in which drainage is provided at both the top and bottom of the specimen. The measurement of pore pressure at the bottom of the specimen is facilitated by an o-ring seal at the bottom of the specimen ring, and a porous stone at the bottom that is smaller than the specimen and is contained entirely within the o-ring seal. A hole drilled through the bottom of the consolidometer is attached to an electrical resistance strain gauge piezometer. The hole and bottom porous stones are pre-saturated prior to placement of the specimen. When a load increment is imposed on the top cap, data is recorded simultaneously from the LVDT and piezometer.

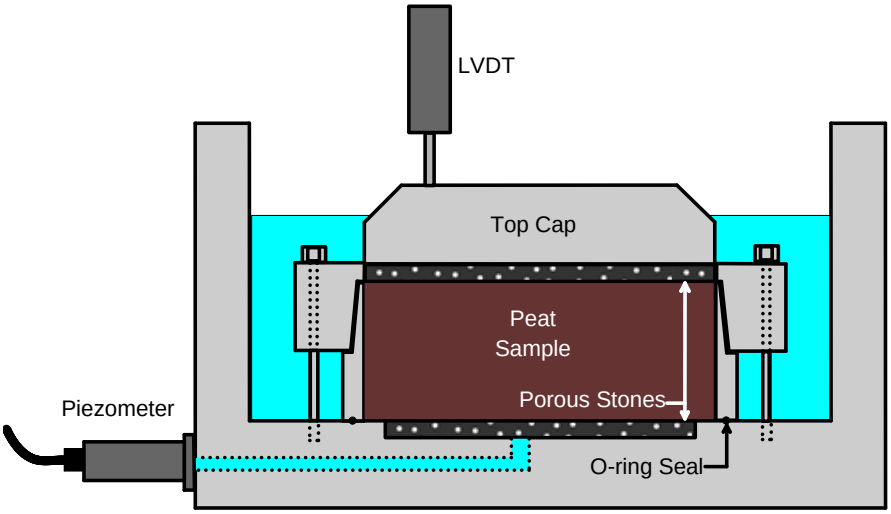

Figure 3.4. Single-drainage consolidometer that permits pore pressure measurement at bottom of specimen.

An example figure showing data collected using the new consolidation device is shown in Fig. 3.5. In this particular case, a peat sample with an organic content of 51% is loaded from an initial vertical effective stress of 38 kPa to a final vertical effective stress of 75 kPa. The pore pressure increases slowly from about 0 to 5 kPa from approximately 0.1s to about 8s. The change in pore pressure is less than the change in vertical total stress because the peat is not completely saturated. Lack of saturation also explains the slow increase in pore pressure (the vertical total stress change occurred during a fraction of a second; not over 8 seconds). The pore pressure then dissipates from 8s to about 280s, when it returns to approximately 0. The pore pressure continues to decrease below zero after consolidation finished, which is likely caused by evaporation of water from the chamber. Although the pore pressure reading provides a clear indication of the end of consolidation, the LVDT reading (represented here as void ratio rather than displacement) does not show the characteristic “break” in the curve that is traditionally interpreted as the end of primary consolidation in typical consolidation tests. These data clearly demonstrate the benefit of making the pore pressure measurement for the purpose of accurately defining t_p, even though the pore pressure reading may not be entirely representative of pore pressures within the specimen due to lack of saturation.

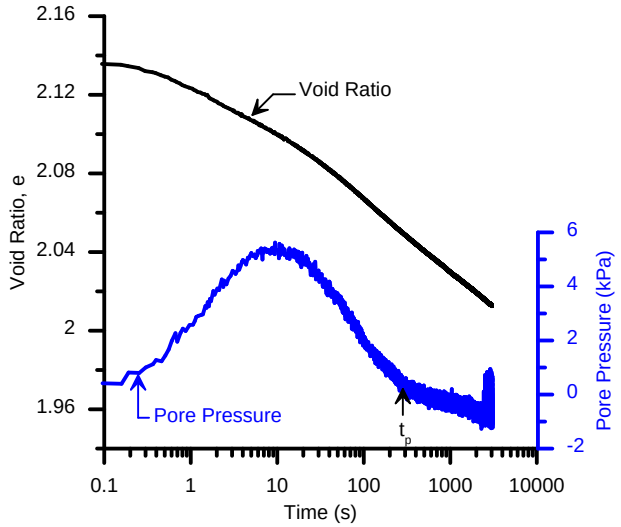

Figure 3.5 Sample data from consolidation device in Fig. 3.4 that clearly shows why pore pressure measurement is necessary for determining end of primary consolidation.

3.5.2 Summary of consolidation tests performed using new consolidometer

Consolidation tests using the new device are ongoing at the time of writing this report. We present the results of three tests as summarized in Table 3.2. All three tests were conducted on samples reconstituted from peat taken from near the surface at Sherman Island, and the organic content is about 50%. This peat was taken from a desiccated crust layer, and has more mineral constituents than peat deeper in the profile, where organic contents approach 70%. Furthermore, the peat has an amorphous structure, with very little fibrous material. The specimens were prepared by mixing the peat as a slurry, placing in a Shelby tube, and pre-consolidating to approximately 8 kPa. The specimens were subsequently extruded from the Shelby tube into the consolidometer ring, trimmed, and placed in the consolidometer. Blank spaces in Table 3.2 indicate that the test terminated before reaching that particular load stage. Furthermore, the initial effective stress at the beginning of the first load stage is unknown because of the potential for matric suction in the soil. The specimens were initially not externally loaded at the beginning of stage 1, but negative pore pressure in the specimens may have contributed to maintaining some unknown amount of effective stress. At the end of the first stage, and at the beginning and end of subsequent load stages, the effective stress is known. Following application of the stage 1 loads in tests 1 and 2, small load increments were imposed for the purpose of identifying how large a load increment must be to begin resetting the secondary compression clock (discussed later).

Test 3 is a more traditional consolidation test in which the load increment is doubled for each stage.

Table 3.2. Summary of consolidation tests performed using the new consolidation device.

	Test 1			Test 2			Test 3		
Stage	σ_{vo}' (kPa)	σ_{vf}' (kPa)	$\Delta\sigma_v$ (kPa)	σ_{vo}' (kPa)	σ_{vf}' (kPa)	$\Delta\sigma_v$ (kPa)	σ_{vo}' (kPa)	σ_{vf}' (kPa)	$\Delta\sigma_v$ (kPa)
1	?	9.3	?	?	18.7	?	?	9.3	?
2	9.3	9.5	0.2	18.7	19.1	0.5	9.3	18.7	9.3
3	9.5	10.0	0.5	19.1	20.2	1.1	18.7	37.4	18.7
4	10.0	11.0	1.0	20.2	22.6	2.4	37.4	74.6	37.3
5	11.0	13.4	2.4	22.6	27.2	4.6	74.6	149.2	74.6
6	13.4	17.4	3.9	27.2	35.2	8.0	149.2	298.2	149.0
7	17.4	24.9	7.6	35.2	49.0	13.8			
8	24.9	37.7	12.8	49.0	73.7	24.7			
9	37.7	75.0	37.2						

3.5.3 Measured values of secondary compression index, C_α

Results from Test 3 are shown in Fig. 3.6. The consolidation curve identifies that the peat was normally consolidated, which was independently known since we tested a reconstituted specimen. Note that the first load increment of 9.3 kPa was higher than the consolidation stress of 8 kPa used to create the specimen. The slope of the e vs. log(σ'_{vc}) line, defined as the virgin compression index, is C_c = 0.4. Also shown in Fig. 3.6 is the relation between secondary compression index, C_α, and consolidation stress, σ'_{vc}. This relation clearly shows that secondary compression index increases as consolidation stress increases. The fundamental mechanism controlling this behavior is not known, and we also do not know whether a similar trend exists for other soil types (i.e., clay) or whether this behavior is specific to this peat material. Nevertheless, the trend is very clear and selecting C_α to be consistent with σ'_{vc} is likely important for many problems.

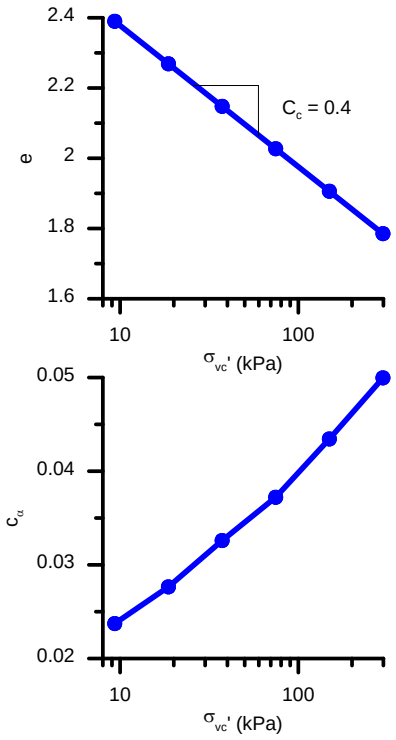

Figure 1.6 Consolidation curve showing e vs. σ'_{vc}, and relation between secondary compression index and σ'_{vc}.

3.5.4 Interpreting the resetting of secondary compression clock

In the previous section, we demonstrated that identifying the break in the dial gauge reading versus log-time plot is difficult for peat. In this section we demonstrate that the traditional procedure, in which t=0 corresponds to the time when the load is applied, is inappropriate for small load increments and we suggest a new interpretation framework based on resetting of the secondary compression clock by an amount that is proportional to the volumetric strain caused by primary consolidation. Tests 1 and 2 were conducted specifically to study resetting of the secondary compression clock.

To first demonstrate that the traditional procedure doesn't work well for small load increments, consider a test on the same specimen shown in Fig. 3.5, but for a different load stage in which a 9.3 kPa vertical stress increment is imposed first (Stage 1), followed by a very small 0.2kPa load increment (Stage 2). Fig. 3.7 shows the results recorded from this test plotted with

t=0 corresponding to the beginning of Stage 1. The load increment imposed in Stage 2 is so small that only a very small change in void ratio due to consolidation is apparent immediately after load application. The slope of the secondary compression line increases very slightly from Stage 1 to Stage 2. This makes sense because the loading imposed during Stage 2 was so small that it had very little influence on the soil fabric, and on the factors that control secondary

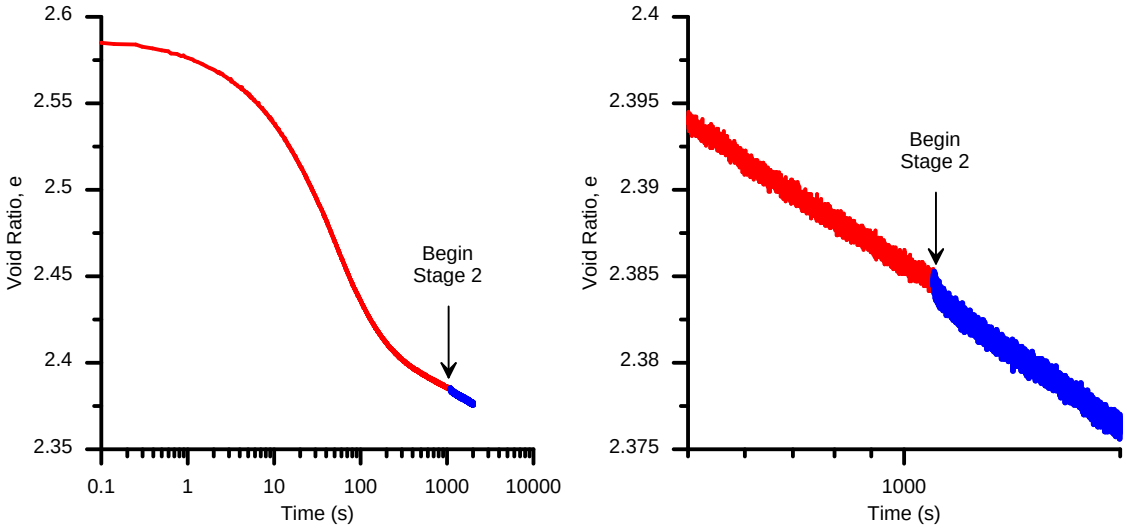

Figure 3.7. Consolidation test on peat specimen with 51% organic content. In Stage 1, a vertical load increment of 9.3 kPa was imposed on an initially unloaded specimen, and in Stage 2, an additional 0.2 kPa load increment was imposed.

Although the data presented in Fig. 3.7 make sense, this presentation of the Stage 2 data is a violation of the traditional procedure in which the clock is reset at the time of load application. The Stage 2 data from Fig. 3.7 is plotted again in Fig. 3.8, except that the clock is reset at the time when the load is applied at the beginning of Stage 2 (i.e., Stage 2 is started approximately 1050 seconds after Stage 1 was started, so 1050 seconds was subtracted from the Stage 2 data in Fig. 3.7). Bearing in mind that excess pore pressure dissipated after only a few seconds, we would expect this plot to be essentially linear since the change in void ratio is controlled by secondary compression. However, plotted in the traditional manner in which the clock is reset when the load is applied, the secondary compression behavior exhibits a nonlinear trend with slope increasing over time. The explanation for this behavior is very simple: the clock should not have been reset at the start of Stage 2 because the load increment is so small. This illustrates that the concept of secondary compression involves a specific reference time at which the secondary compression clock is reset by a large load increment that induces significant strains, and using

the incorrect reference time results in nonlinear void ratio versus log-time behavior. This explanation is clearly demonstrated in Fig. 3.7 because the slope of the secondary compression line did not change much after imposing the small load increment in Stage 2, therefore the reference time for Stage 2 must be close to the beginning of Stage 1. A secondary compression slope, C_α, cannot be accurately derived from Fig. 3.8, therefore we conclude that the traditional procedure for interpreting secondary compression cannot be applied to small load increments.

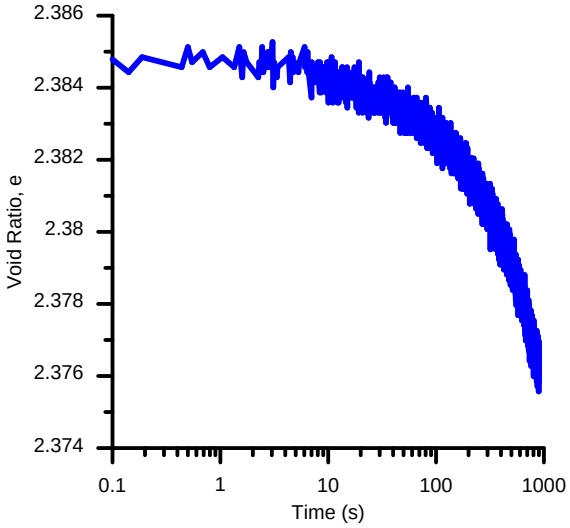

Figure 3.8. Void ratio versus time for the Stage 2 data plotted in Fig. 3.7, except with the clock reset at the time of application of the 0.2 kPa load increment.

A data interpretation procedure was developed to compute the reference time for secondary compression based on recorded consolidation test data. Equation (3.1) defines an expression for secondary compression assuming that t=0 corresponds to the beginning of a particular load stage, and t_{ref} corresponds to the reference time for the secondary compression clock, and is less than zero for cases where the secondary compression clock is not completely reset, and equal to zero for cases where the secondary compression clock is completely reset. This equation corresponds to the condition depicted in Fig. 3.9 in which the secondary compression clock started at some time before the start of the load stage.

$$e_p - e = c_\alpha \log\left(\frac{t - t_{ref}}{t_p - t_{ref}}\right) \quad t > t_p \tag{3.1}$$

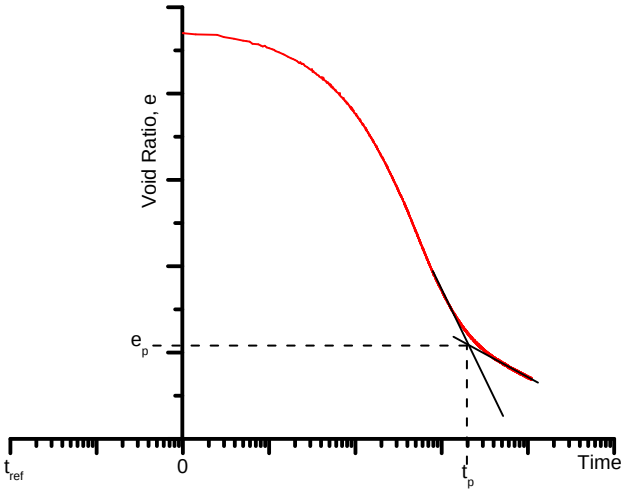

Figure 3.9. Void ratio versus time for the Stage 2 data plotted in Fig. 3.7, except with the clock reset at the time of application of the 0.2 kPa load increment.

In Eq. (3.1), we assume that C_α is a known constant that depends on σ'_{vc} as shown in Fig. 3.6, and is equal to the value of C_α that would be measured if the secondary compression clock were to completely reset for a particular load stage. If we measure the void ratio, e, as a function of time during a time interval following primary consolidation (i.e., $t > t_p$), the reference time can then be computed by linear least-squares regression by rearranging Eq. (3.1) as shown in Eq. (3.2), where $\boldsymbol{t}$ and $\boldsymbol{e}$ are the vectors of measured values after the end of primary consolidation and $t = 0$ represents the start of the load stage.

$$\underbrace{\left(10^{\frac{e_p - e}{C_\alpha}} - 1\right)}_{X} \cdot t_{ref} = \underbrace{t_p \cdot 10^{\frac{e_p - e}{C_\alpha}} - t}_{Y} \qquad (3.2)$$

$$t_{ref} = \left(X^T X\right)^{-1} X^T Y$$

Equation (3.2) was applied to interpret the data shown in Fig. 3.10 for Test 1 and Test 2, and values of t_{ref} were computed for each case. A dimensionless index was formulated to indicate the percentage by which each load stage reset the secondary compression clock:

$$\theta_i = \frac{\Delta t_{ref,i} + \left(t_{ref}\right)_i}{\Delta t_{ref,i}} \tag{3.3}$$

where θ_i is the reset index for the i^{th} load stage, $(t_{ref})_i$ is the reference time for the i^{th} load stage, and $\Delta t_{ref,i}$ is the time elapsed between t_{ref} for the previous load stage, $(t_{ref})_{i-1}$, and the onset of loading for stage i. In 3.3, $\Delta t_{ref,i}$ is greater than or equal to zero and t_{ref} is less than or equal to zero. Note that if θ =0, the secondary compression clock is not reset at all [i.e., $(t_{ref})_i = \Delta t_{ref,i}$], and if θ =1 the secondary compression clock completely resets because $(t_{ref})_i$ is zero while $\Delta t_{ref,i}$ is finite.

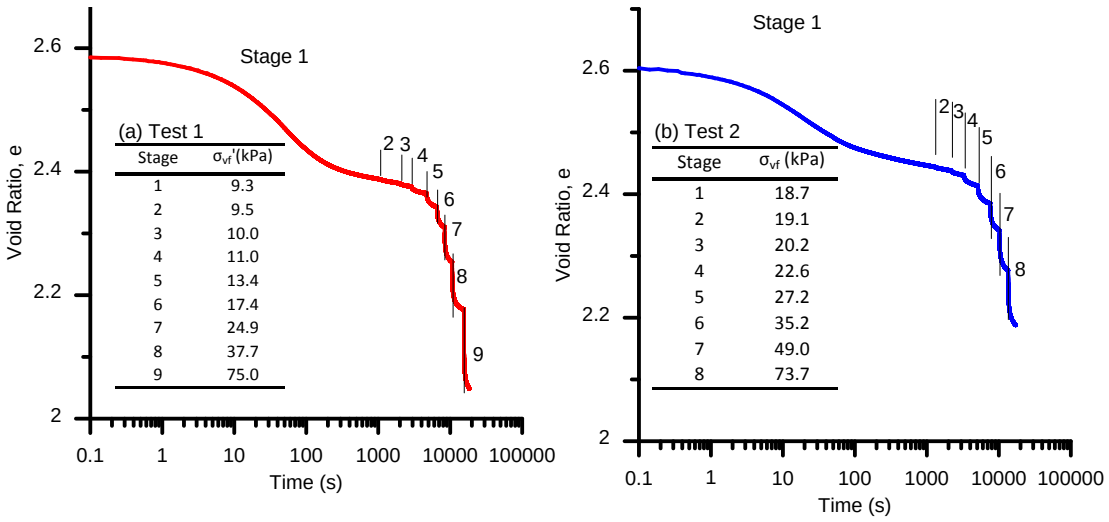

Figure 3.10. Void ratio versus time for (a) Test 1, and (b) Test 2.

Values of θ were computed for each load stage, and plotted against the volumetric strain induced by primary consolidation for that load stage, $\varepsilon_{v,pc}$, as shown in Fig. 3.11. The value of $\varepsilon_{v,pc}$ was computed based on the known value of C_c = 0.4 because the very small changes in dial gauge reading were difficult to interpret for small load stages [i.e., $\varepsilon_{v,pc} = C_c \log(\sigma'_{vf} / \sigma'_{v0}) / (1+e)$]. A very interesting trend emerges from these data. When the value of $\varepsilon_{v,pc}$ is less than about 0.1%, the secondary compression clock is not reset at all. This

can be considered as a threshold volumetric strain for secondary compression reset. When the value of $\varepsilon_{v,pc}$ is above about 1%, the secondary compression clock is completely reset. A linear trend between these two threshold values appears to fit the data reasonably well, as indicated by the dashed line.

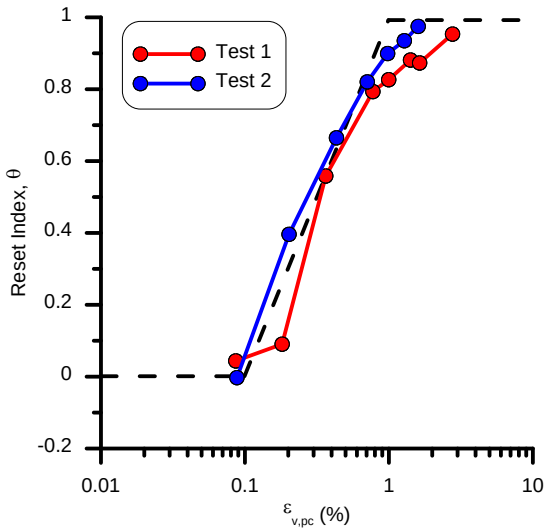

Figure 3.11 Secondary compression reset index, θ, versus volumetric strain induced by primary consolidation, ε_{vc}.

3.6 CYCLIC SHEAR TESTING OF PEAT SPECIMENS

3.6.1 Test results

Undrained strain-controlled cyclic direct simple shear (DSS) and cyclic triaxial (CTX) tests with post cyclic volume change measurements were conducted using the staged process described in Section 3.3. As shown in Table 3.1, we have performed eight such test sequences on specimens from the 1.3-3.0 m depth range. Following undrained cyclic shear, triaxial specimens were consolidated over time intervals of 20 min (specimens 8-3c and 8-3d) and 24 hrs (specimen 9-3a). Direct simple shear specimens were consolidated for 22 min. Specimens with longer post-shear consolidation time experience a large fraction of their volume change from secondary compression; we seek to investigate the effect of prior cyclic loading on secondary compression behavior.

Figures 3.12 and 3.13 show results of typical DSS and CTX test sequences (reconstituted specimen for DSS, $\sigma'_{vc} = 15kPa$ and 9-3a for CTX, $\sigma'_{vc} = 42kPa$) respectively. During cyclic loading, pore pressure ratio $r_u = \Delta u/\sigma'_{vc}$ increases and the soil stiffness degrades as evidenced by reductions in the shear stress to achieve the uniform strain amplitude. Figure 3.14a shows for each sequence of shearing the residual pore pressure at the end of cycle 15, which we denote r_{ur}, as a function of the shear strain amplitude (γ_c). The pore pressure generation markedly increases for cyclic strain amplitudes larger than 0.5-1.0% and tend to be higher for the DSS shearing than in the CTX shearing. The largest observed pore pressure ratios were in the range of 0.6-0.8 for DSS testing and 0.2-0.4 for CTX testing. These values are lower than those for liquefiable sands but are comparable to those for cyclic softened normally consolidated clays (e.g., Boulanger and Idriss, 2007). The larger pore pressures from the DSS versus the CTX stress paths follows expected patterns of behavior from prior work (Seed and Peacock 1971, Finn et al. 1971, Boulanger, 2003), and can be attributed to the rotation of principal stresses in DSS tests, which is absent in CTX tests. The rotation of principal stresses produces a stronger effect of stress reversal on the specimens, thus more rapidly degrading the soil structure. The difference is likely also partially attributed to the fact that the triaxial specimens were not completely saturated, therefore undrained loading conditions could not be achieved even with the drain taps closed, whereas equivalent undrained conditions were achieved in simple shear by enforcing constant volume conditions during shear.

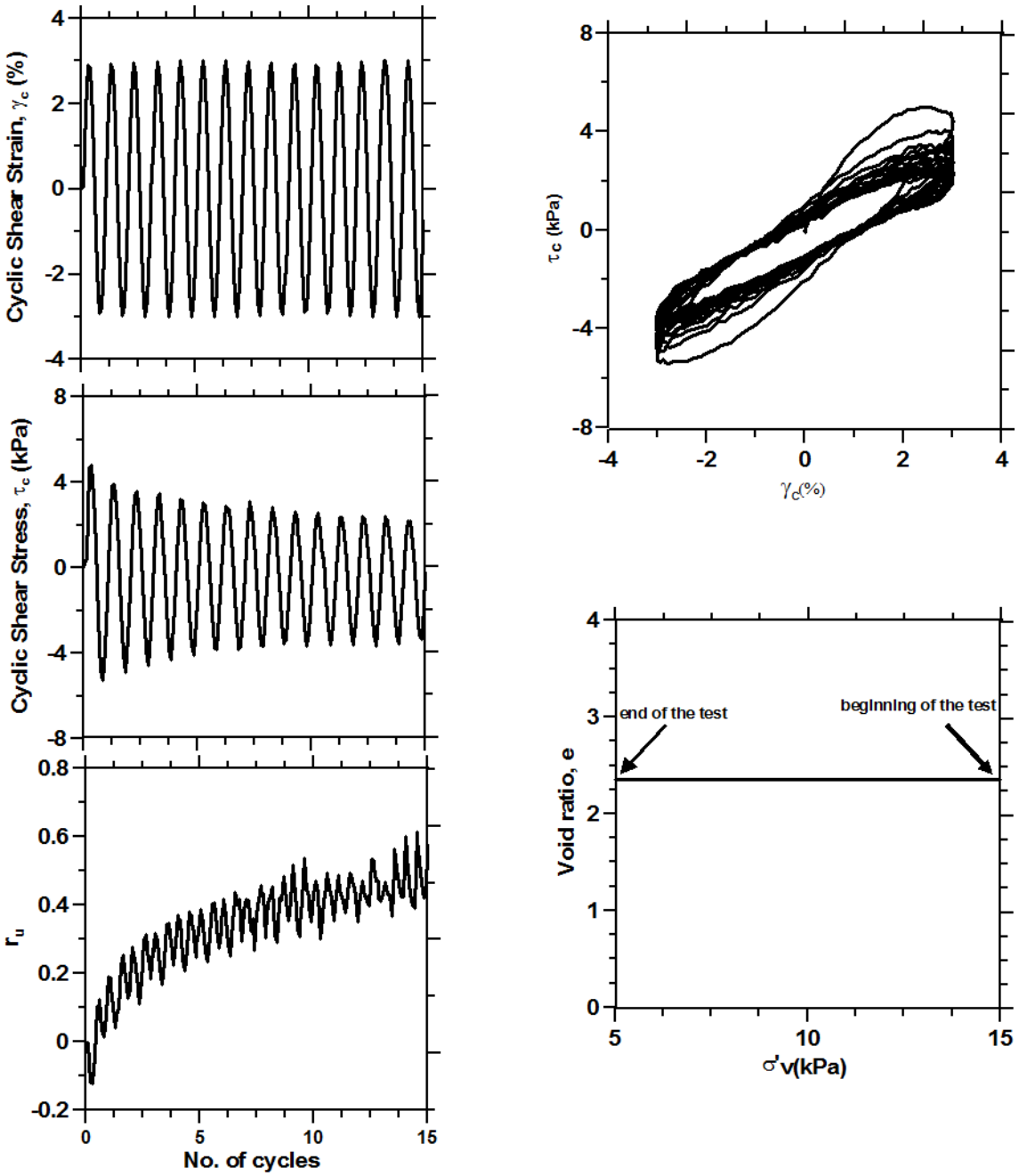

Figure 3.12. Cyclic behavior of a reconstituted specimen (organic content=51%) under cyclic loading in UCLA-DSS device.

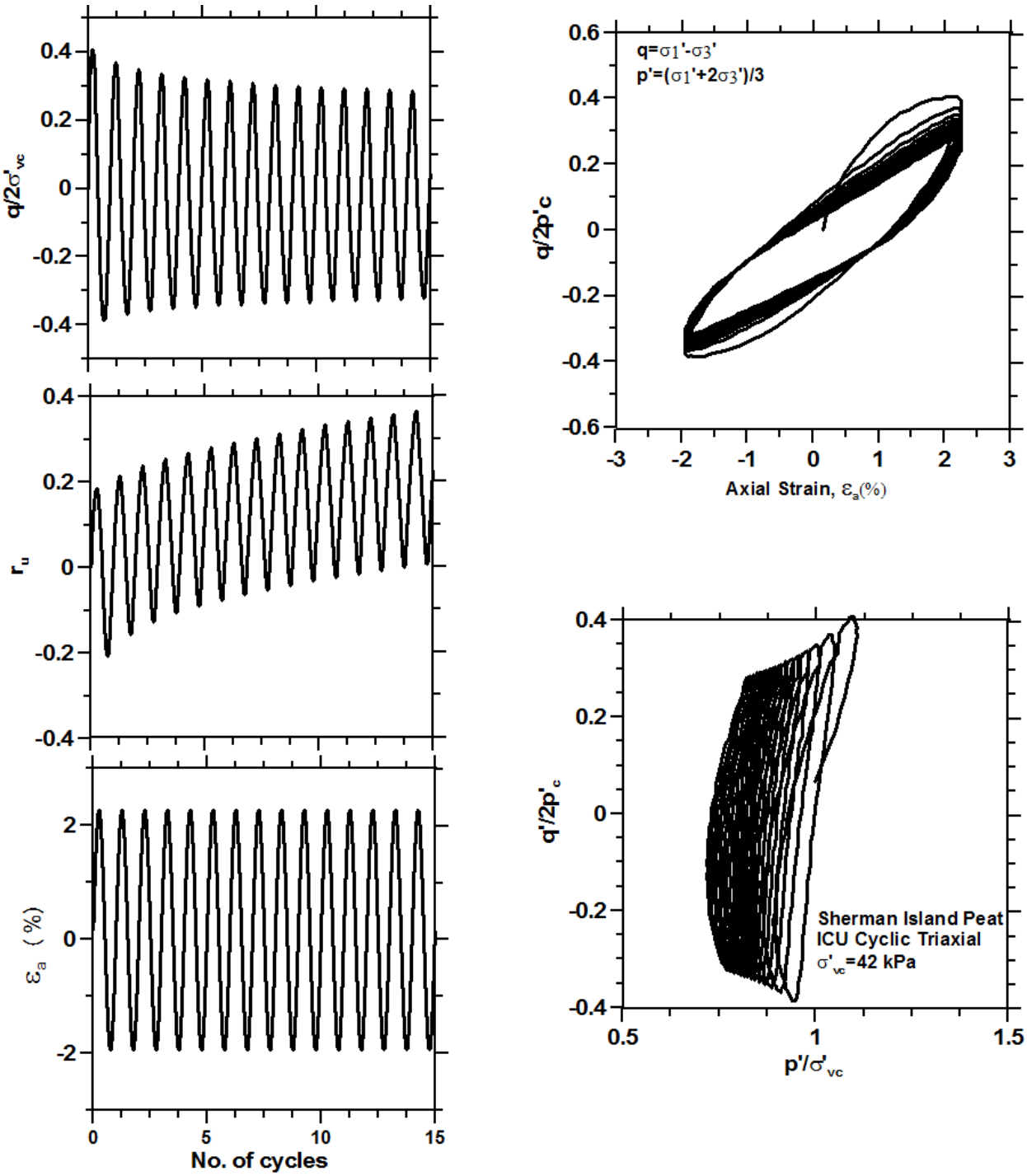

Figure 3.13. Cyclic behavior of specimen 9-3a under cyclic loading in CTX device.

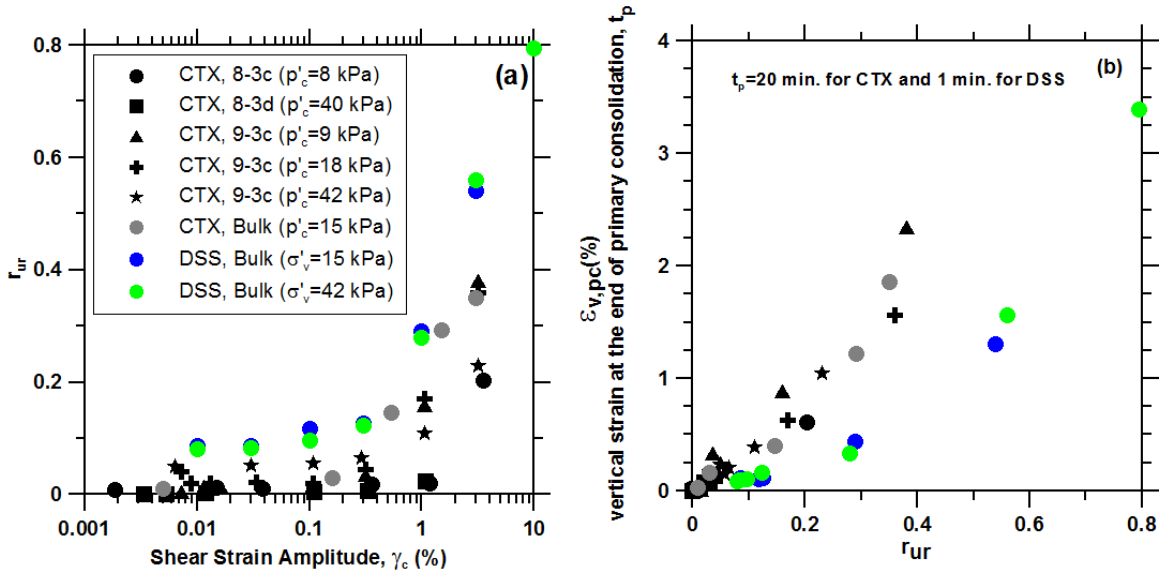

Figure 3.14. Post-cyclic behavior of the tested peat (a) residual pore pressure, and (b) post-cyclic volume change at end of primary consolidation (t_p).

Following the end of cyclic loading, volume change was allowed by restoring the original vertical load on DSS specimens or the drain valve was opened in CTX specimens and post-cyclic volumetric strain was monitored as a function of time. Figure 3.14b shows the vertical strain ($\varepsilon_{v,pc}$) at the end of primary consolidation (t_p), which was judged to be 1200 s (20 min) in the CTX tests and around 1 min in the DSS tests, as a function of r_{ur}. The difference between t_p of DSS and that of CTX can be attributed to the difference in their drainage path lengths as the specimen height in the DSS is almost 1/5 of CTX's. Interestingly, although more pore pressure is developed in the DSS with respect to CTX (Fig. 3.14a), less $\varepsilon_{v,pc}$ is observed in the DSS comparing with CTX (3.14b). The difference between the volume changes can be attributed to the creep which occurs simultaneously with primary consolidation, and hence, to get better understanding of volume change behavior, both DSS and CTX results should be plotted at an identical post-cyclic time period, as will be explained in Section 3.6.1. In addition, it is observed that $\varepsilon_{v,pc}$ is much more strongly correlated with r_{ur} than with γ_c. The relationship with r_{ur} is expected because this volume change is associated with primary consolidation that dissipates the excess pore pressures. We verify this hypothesis by computing the theoretical volume change associated with recompression over the stress increment produced by pore pressure generation:

$$\varepsilon_{v,pc} = \frac{C_r}{1+e_0}\log\left(\frac{1}{1-r_{ur}}\right) \tag{3.4}$$

where e_o is the soil void ratio at the start of post-cyclic consolidation. The results of this calculation for DSS specimens are shown in Fig. 3.15, which shows an excellent match to the observed volumetric strain data attributed to primary consolidation (i.e., 1 min).

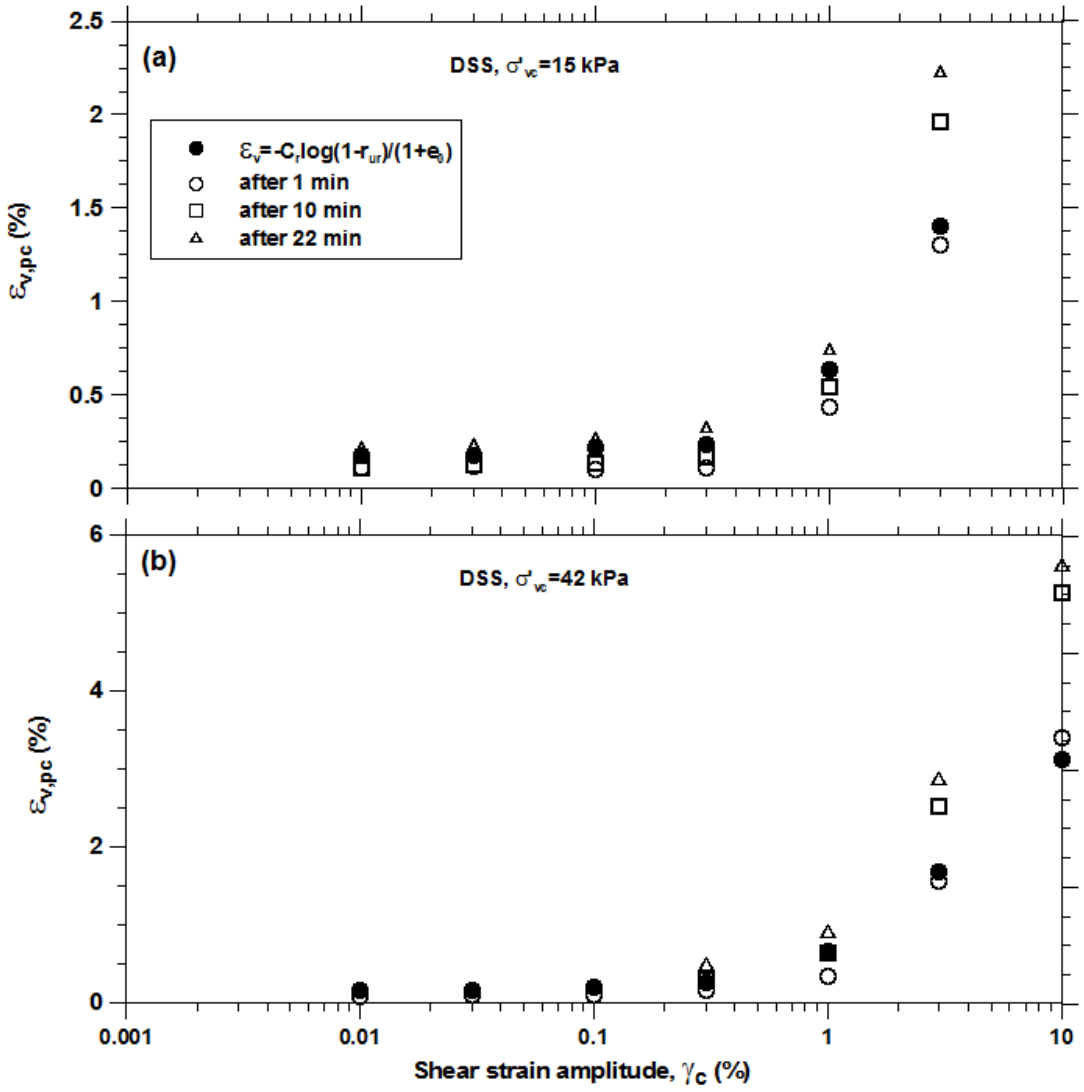

Figure 3.15. Post-cyclic volume change from primary consolidation

3.6.2 Resetting of secondary compression clock due to cyclic shearing

As indicated in Table 3.1, most the test specimens considered in this work were allowed to undergo volume change for times beyond t_p. Volume change that occurred for $t > t_p$ is attributed to secondary compression, although we recognize that some fraction of the volume change that occurs during $t < t_p$ is likely also affected by secondary compression. By examining the varying levels of volume change from secondary compression for different shear strain amplitudes (γ_c) and developed pore pressures (r_{ur}), we investigate the effects of cyclic shearing on post-cyclic secondary compression.

We quantify the post-cyclic secondary compression in a framework similar to what explained in Section 3.5.4. Figure 3.16 shows two examples of post-cyclic volume changes measurements, one (Fig. 3.16a) following an increment of small-amplitude cyclic straining ($\gamma_c = 0.03\%$) and one (Fig. 3.16b) following an increment of large-amplitude shaking ($\gamma_c = 3\%$). Figure 3.16a is similar to Fig. 3.8, stating that if the level of cyclic shear strain is low, the clock for the secondary compression will not be fully reset.

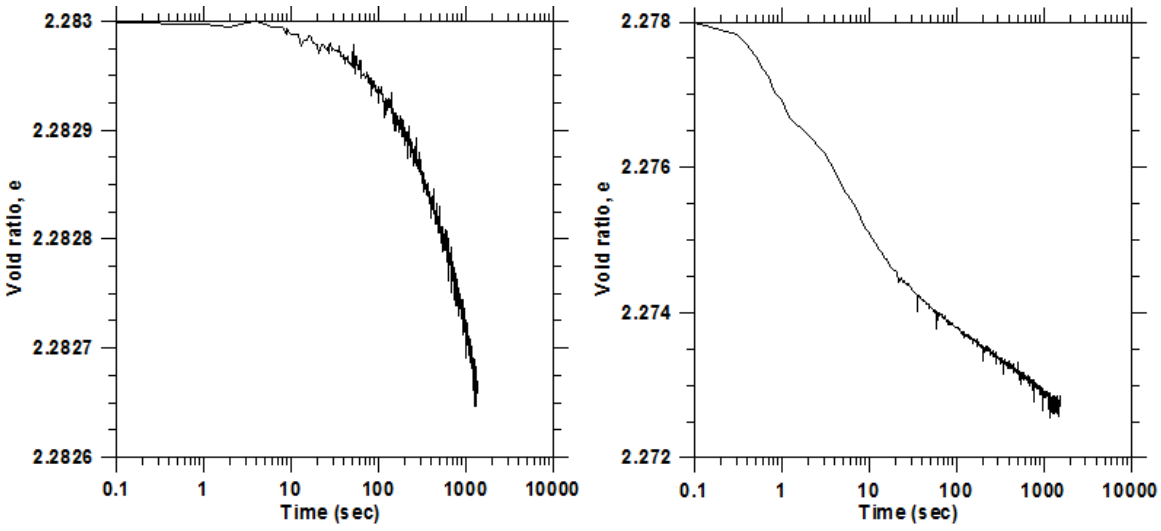

Figure 3.16. Post-cyclic volume change for a DSS test conducted on a reconstituted specimen (organic content=51%), $\sigma'_{vc} = 15kPa$ **(a)** $\gamma_c = 0.03\%$ **(b)** $\gamma_c = 3\%$

To quantify how much each load stage reset the secondary compression clock, we followed the procedure explained in Section 3.5.4, and found the values of reset index, θ for a series of tests at different shear strain amplitudes. In Figure 3.17, we relate θ to cyclic shear strain

amplitude (Fig. 3.17a), residual pore pressure ratio (Fig. 3.17b), and post-cyclic volume change from primary consolidation (Fig. 3.17c) for a DSS test conducted on a reconstituted specimen (organic content=51%), $\sigma'_{vc} = 15kPa$. The data show that the secondary compression clock is partially reset in this sequence of tests, but that full re-setting is not achieved. The strongest predictors of re-setting (i.e., the quantities producing the steepest slopes in the plots) are r_{ur} and $\varepsilon_{v,pc}$. We observe that resetting does not occur for r_{ur} < ~0.08 or $\varepsilon_{v,pc}$ < 0.1%. We see $\theta > 0.7$ for $r_{ur} > 0.3$ or $\varepsilon_{v,pc} > 0.4$%.

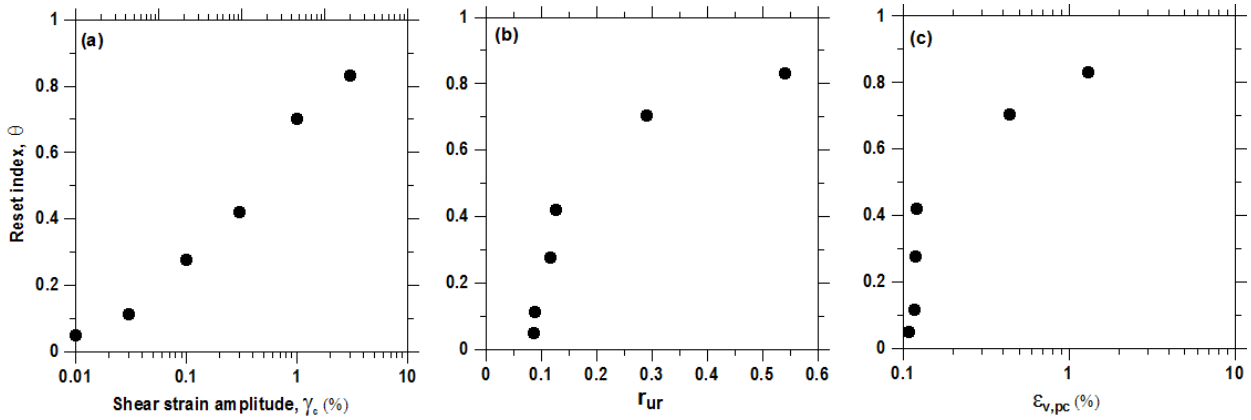

Figure 3.17 Reset index for a DSS test conducted on a reconstituted specimen (organic content=51%), $\sigma'_{vc} = 15kPa$ in terms of (a) cyclic shear strain amplitude, (b) residual pore pressure ratio, and (c) post-cyclic volume change from primary consolidation.

Having now determined the influence of cyclic shearing on secondary compression behavior, we can return to Fig. 3.14b, which showed that for a given excess pore pressure ratio, the cyclic triaxial tests exhibited more volume change than the simple shear tests at the end of primary consolidation. Recall that the end of primary consolidation occurred more quickly during the simple shear tests than for the triaxial tests (i.e. after about 1min compared with 20min) due to the shorter drainage path length, therefore less secondary compression occurred during consolidation for the DSS tests than for the CTX tests. Once the values of θ were computed for each load stage, we estimated the amount of secondary compression that would occur from 1min to 22min for DSS tests, and the results are shown in Fig.3.18. Following this correction, the relationship between r_{ur} and $\varepsilon_{v,pc}$ after 22 minutes is consistent for the two stress paths, which confirms the hypothesis that secondary compression occurring simultaneously with primary consolidation was responsible for the higher volumetric strains measured in the triaxial testing

device. This result also shows that while the stress paths associated with DSS may induce more pore pressure than CTX for a given level of shear strain, there is a practically identical volume change for both test types conditional on a given r_{ur}.

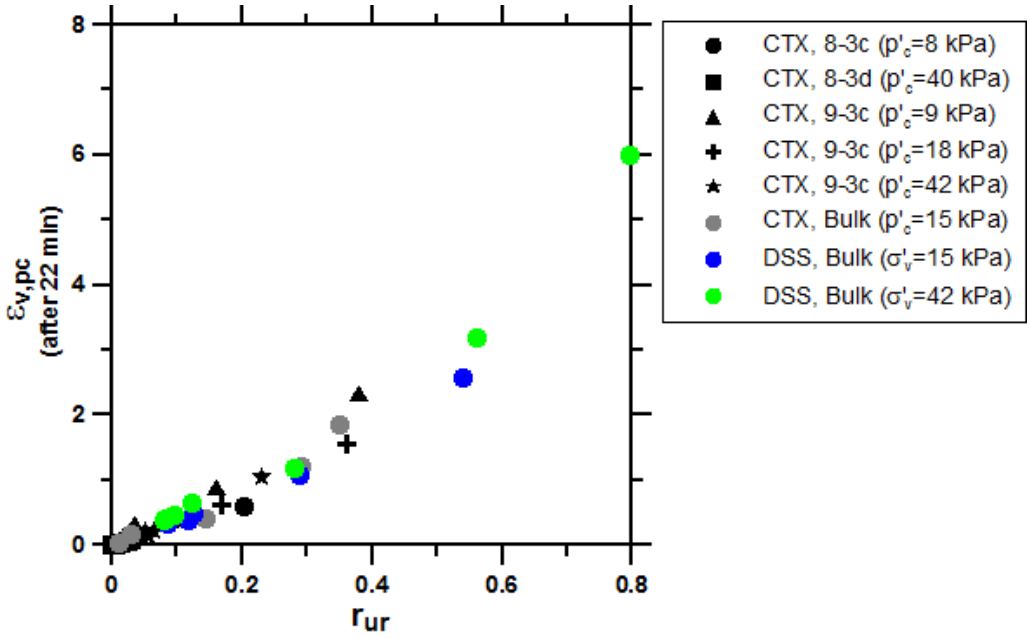

Figure 3.18. Post-cyclic volume change after 22 min corrected for the effect of creep

3.7 IMPLICATIONS OF SECONDARY COMPRESSION CLOCK RESETTING FOR LEVEES FOUNDED ON PEAT

The concept of resetting of the secondary compression clock is potentially very important for levees founded on peat soil because the excess pore pressures generated by cyclic shearing may only partially reset the secondary compression clock. Furthermore, settlement of levees on peat is dominated by secondary compression, with primary consolidation playing a relatively minor role. This is clearly an important issue to study in more detail, and additional work is required to relate the amount by which the secondary compression clock resets to the amount of remolding that occurs during a particular load sequence. Relations such as those shown in Fig. 3.11 and 3.17 are needed for a broad range of organic content to more clearly define relations for the range of soil conditions of interest.

4 Summary and Future Work

4.1 SUMMARY

There are two major components to the work performed as part of this project. The first involves improvements of a simple shear testing device to enable constant volume testing. The second component involves the application of this and other devices for testing of peaty organic soils to investigate their tendency to develop pore pressures during cyclic loading and the effect of the pore pressure generation on shear strength and post-cyclic volume change.

We have adapted an existing state-of-the-art digitally controlled simple shear device, originally designed for drained testing, to perform constant height testing. The control requirements associated with constant height testing required substantial re-design of the control system. The new system utilizes PID control of horizontal displacements coupled with either vertical force control (for drained testing in which volume change is allowed; vertical force is maintained constant in this case) or vertical displacement control (for constant volume testing; vertical displacement is held constant in this case). We demonstrate that the new system has substantially similar control capabilities for horizontal displacement as the earlier control system. We show that the level of vertical control achieved during constant height testing is excellent in several respects – the levels of height change are very small (less than 0.05% of the specimen height for large shear-strain tests) and are maintained even at relatively high frequencies. This level of vertical control, especially at high frequencies, has not been possible in prior simple shear devices. Moreover, rocking of the top cap is shown to be similarly small, with the height change due to rocking at the specimen edge being half or less than that from imperfect vertical control. To our knowledge, this is the first such documentation of device performance with respect to rocking.

We investigate through laboratory testing the volume change characteristics of peaty organic soil from Sherman Island, California under static conditions (consolidation, secondary

compression) and under cyclic and post-cyclic conditions from cyclic triaxial (CTX) and cyclic direct simple shear (DSS) testing. Incremental consolidation tests indicate the material to be highly compressible (C_c = 0.4, C_r = 0.1) and prone to substantial ageing from secondary compression (C_α/C_c = 0.06-0.07 following virgin compression). Careful examination of the consolidation test data shows an important, and rather fundamental, aspect of secondary compression, which is that its characteristic feature of occurring at an exponentially decaying rate following load application is not universal. Rather, that "classical" behavior occurs only following stages of loading that produce at least 3% vertical strain. On the other hand, for smaller load increments, the secondary compression rate following the addition of load is relatively modest, and in the extreme may not depart from what occurred prior to load application. We proposed a simple model to characterize this effect that is based on inference of a 'resetting' time for secondary compression.

From strain-controlled cyclic triaxial and simple shear testing of peaty organic soil from Sherman Island, we find the generation of cyclic pore pressures to increase markedly for cyclic shear strain levels beyond approximately 0.5-1.0%, with the largest residual pore pressure ratios r_{ur} (cyclic residual pore pressure normalized by pre-cyclic consolidation stress) being approximately 0.6-0.8 for DSS testing and 0.2-0.4 for CTX testing. For a given level of shear strain, we find larger pore pressures from DSS testing than for CTX testing, which we attribute to the rotation of principal stresses that is present in DSS and absent in CTX. Post-cyclic volume change occurs from pore pressure dissipation and secondary compression. The level of post-cyclic primary consolidation appears to be uniquely related to the recompression index of the soil and r_{ur}. The secondary compression following cyclic loading is well explained by the proposed resetting model. Significantly, this work shows that when large cyclic shear strains occur in peaty organic soil, they cause pore pressure ratios that are not large enough to significantly degrade shear strength, but which are large enough to partially re-set the secondary compression process. This enhancement of secondary compression, in turn, could lead to settlements of levees founded on such materials that could produce catastrophic loss of freeboard. These possible failure mechanisms are not considered in existing hazard assessments for regions such as the California Bay-Delta region, and will need to be explored in future work.

4.2 FUTURE WORK

This report has presented a limited amount of laboratory data that clearly demonstrates that peat soil exhibits post-cyclic volumetric strain due to primary consolidation associated with dissipation of excess pore pressure and an increase rate of secondary compression due to resetting of the secondary compression clock. Post-cyclic volume change is a previously unidentified mechanism that may have significant influence on seismic levee design standards in places where levees are founded on peat, such as in the Sacramento / San Joaquin Delta. Additional research is required to (1) fully flesh out the framework set forth in this report so that it is applicable over the range of conditions encountered in field conditions (e.g., organic content, consolidation stress, overconsolidation ratio, etc.), (2) develop a simple procedure that design engineers can use to predict post-cyclic settlement of levees on peat soil, and (3) develop a constitutive model that can be utilized in a nonlinear numerical simulation (e.g., finite element or finite difference analysis). We have secured funding to continue working toward these goals from the California Department of Water Resources (DWR) and the National Science Foundation, and briefly explain our future plans in this section.

With funding from DWR we plan to perform more cyclic shear tests and consolidation tests of peat samples collected from Sherman Island during a now-completed field testing program in which we shook a model levee resting atop peaty organic soil. These are the same samples we tested as part of this report, but an additional year or so will be required to test the remaining specimens. The organic content of these specimens ranges from about 50% to 80%, covering a wide range of conditions that exist within the Delta. We may also collect samples from more locations in the Delta as part of this study, pending the outcome of coordination with DWR on the scope of work and contract details. We plan to perform primarily strain controlled simple shear tests with post-cyclic consolidation measurements, stress controlled simple shear tests to study strength degradation for stability calculations, and consolidation tests to further refine the secondary compression clock resetting mechanism.

From the DWR study, we will develop simple procedures that engineers can use to predict post-cyclic settlement of levees on peat soil. We envision that this will involve the following steps: (1) estimate a representative shear strain amplitude and number of representative cycles for a particular levee and seismic scenario, (2) compute the amount of excess pore pressure anticipated for the loading conditions in step 1, (3) compute the amount of primary consolidation

based on the recompression index of the soil beneath the levee, (4) compute the amount of resetting for the secondary compression clock using the resetting index approach developed in this report, and (5) plot a settlement versus time graph that combines primary consolidation and secondary compression. We anticipate that steps (2), (3), and (4) of this procedure will be developed entirely from laboratory test data. Users will have the option of performing their own testing on soils beneath the levees, or using the recommended relationships measured from our laboratory test program. We anticipate that step (1) will require an evaluation of levee-peat interaction to develop estimates of shear strain beneath various regions of the levee, which is a topic of study of our NSF-funded study explained in the next paragraph.

From the NSF study, we plan to develop a constitutive model for peat that is based on critical state soil mechanics concepts, and will be an updated version of the Cam Clay model that accounts for secondary compression including clock resetting. This work is underway, and we are currently focusing on developing a hardening law formulated in the bounding surface plasticity framework that adequately matches the modulus reduction and damping behavior of the peat. The laboratory testing presented in this report and future laboratory tests will be utilized to help develop the constitutive model. Once the model is developed, we plan to run nonlinear dynamic simulations to assess the post-cyclic volume change potential of levees resting atop peat soil. We will supplement these nonlinear simulations with elasto-dynamic simulations intended to characterize the levee-peat interaction mechanism that arises from the levee fill being stiffer than the underlying peat. Such levees may exhibit rocking behavior that rotates principal stress directions beneath various portions of the levee. For example, a rocking levee may introduce significant vertical stress increments in addition to the predominantly simple shear mechanism associated with free-field site response behavior. By contrast, the peat beneath the crest of the levee may be exposed to a stress path the more closely resembles simple shear. This may be important for two reasons: (1) shear strains may be larger beneath the toe than beneath the crest, thereby resulting in more post-cyclic consolidation and secondary compression in these regions, and (2) rotations of principal stresses within the levee fill may result in liquefaction behavior that is not adequately captured by existing evaluation procedures.

In summary, the work performed as part of this USGS-funded research project was crucial for us to prove the concept that peat soil exhibits post-cyclic volume change, and we have been

able to secure additional funding to continue the work and fulfill the overall vision of the research plan.

REFERENCES

ASTM, 2010. *Standard Test Methods for One-Dimensional Consolidation Properties of Soils Using Incremental Loading*, D2435 / D2435M , West Conshohoken, Pa.

Atkinson, J.H. and P.L. Bransby, 1978. *The Mechanics of Soils: An Introduction to Critical State Soil Mechanics*, McGraw Hill, London, UK.

Bjerrum, L. and A. Landva, 1966. Direct simple shear tests on a Norwegian quick clay, *Geotechnique*, 16(1), 1–20.

Boulanger, R.W., 2003. High overburden stress effects in liquefaction analysis, *J. Geotech. Geoenviron. Eng.*, 129 (12), 1071-1082.

Boulanger, R.W., R. Arulnathan, L.F. Harder, R.A. Torres, and M.W. Driller, 1998. Dynamic properties of Sherman Island peat, *J. Geotech. Geoenviron. Eng.*, 124(1): 12-20.

Boulanger, R.W. and I.M. Idriss, 2007. Evaluation of cyclic softening in silts and clays, *J. Geotech. Geoenviron. Eng.*, 133(6), 641-652.

Bro, A.D., J.P. Stewart, and D.E. Pradel, 2013. "Estimating undrained strength of clays from direct shear testing at fast displacement rates," *Geocongress 2013 -- Stability and Performance of Slopes and Embankments III,* San Diego, CA, ASCE Geotechnical Special Publication No. 231, CL Meehan, DE Pradel, MA Pando, and JF Labuz (eds.), Paper No. 5.

CDWR, 1992. Seismic stability evaluation of the Sacramento-San Joaquin Delta levees. Phase I Report: Preliminary Evaluations and Review of Previous Studies, Division of Engineering, California Department of Water Resources (CDWR).

Chu-Chung, H., 2002. Dynamic and cyclic behavior of soils over the wide range of shear strains in NGI-type simple shear testing devices. *PhD Dissertation*, UCLA Civil and Environmental Engineering Department.

Davis, J.H., 1997. The Peat Deposits of Florida, Their Occurrence, Development and Uses. *Geological Bulletin No. 3*, Florida Geological Survey, Tallahassee, FL.

Degroot, D.J., J.T. Germaine, J.T., and R. Gedney, 1991. An electropneumatic control system for direct simple shear testing, *Geotechnical Testing Journal*, 14(4), 339-348.

DRMS, URS Corporation and Jack Benjamin and Associates Inc., 2009. Delta Risk Management Strategy. Phase 1 Final Report. California Department of Water Resources.

Duku, P.M., J.P. Stewart, D.H. Whang, and R. Venugopal, 2007. Digitally controlled simple shear apparatus for dynamic soil testing, *Geotechnical Testing Journal*, 30(5), 1-10.

Duku, P.M., J.P. Stewart, D.H. Whang, and E. Yee, 2008. Volumetric strains of clean sands subject to cyclic loads, *J. Geotech. & Geoenv. Engrg.*, ASCE, 134(6), 1073-1085.

Dyvik , R., T. Berre, S. Lacasse, and B. Raadim, 1987. Comparison of truly undrained and constant volume direct simple shear tests, *Geotechnique*, 37(1), 3-10.

Edil, T.B. and A.W. Dhowian, 1981. At-rest lateral pressure of peat soils, *J. Geotech. Eng. Div.*, ASCE, 107(2), 201-217.

Finn, W.D.L., D.J. Pickering, and P.L. Bransby, P.L. 1971. Sand liquefaction in triaxial and simple shear tests, *J. Soil Mech. & Foundations Div.*, 97(4), 639-659.

Fox, P.J., and T.B. Edil, 1992. C_α/C_c concept applied to compression of peat, *J. Geotech. Eng.*, 118(8), 1256-1263.

Franke, E., M. Kiekbusch, and B. Schuppener, 1979. A new direct simple shear device, *Geotechnical Testing Journal*, 2(4), 190-199.

GeoVision, 2000. Department of Water Resources Boreholes DHP-4D and DHP-5J3 Suspension P&S Velocities. Prepared for California Water Department Resources.

Hanzawa, H., N. Nutt, T. Lunne, Y.X. Tang, and M. Long, 2007. A comparative study between the NGI direct simple shear apparatus and the Mikasa direct shear apparatus, *Soils and Foundations*, 47 (1), 47-58.

Ishihara, K., 1993. Liquefaction and flow failure during earthquakes, *Geotechnique*, 43(3), 351-451.

Ishihara, K. and F. Yamazaki, 1980. Cyclic simple shear tests on saturated sand in multi-directional loading, *Soils and Foundations*, 20(1), 45-59.

Kishida, T., R.W. Boulanger, N.A. Abrahamson, T.A. Wehling, and M.W. Driller, 2009. Regression models for dynamic properties of highly organic soils, *J. Geotech. Geoenviron. Eng.*,133(7), 851-866.

Kjellman, W., 1951. Testing the shear strength of clay in Sweden, *Geotechnique*, 2(3), 225-235.

Ladd, C.C., 1991. Stability evaluation during staged construction, *J. Geotech. Eng.*, ASCE, 117(4), 540-615.

Lowe, J., and T.C. Johnson, 1960. Use of back pressure to increase degree of saturation of triaxial test specimens, *Proc. Research Conference on Shear Strength of Cohesive Soils*, Boulder, Colorado, ASCE, 819-836.

Mesri, G., and M.A. Ajlouni, 2007. Engineering properties of fibrous peats, *J. Geotech. Geoenviron. Eng.*,133(7): 851-866.

Mesri, G., T.D. Stark, M.A. Ajlouni, and C.S. Chen, 1997. Secondary compression of peat with or without surcharge, *J. Geotech. Geoenviron. Eng.*,123(5): 411-421.

Mesri, G., and M.A. Ajlouni, 2007. Engineering properties of fibrous peats, *J. Geotech. Geoenviron. Eng.*,133 (7), 851-866.

Mesri, G., T.D. Stark, M.A. Ajlouni, and C.S. Chen, 1997. Secondary compression of peat with or without surcharge, *J. Geotech. Geoenviron. Eng.*,123(5), 411-421.

Mortezaie, A., and M. Vucetic, 2012. Small strain cyclic testing with standard NGI simple shear device, *Geotechnical Testing Journal*, 35(6), 935-948.

Porcino, D., G. Caridi, M. Malara, and E. Morabito, 2006. "*An automated control system for undrained monotonic and cyclic simple shear tests*," in *GeoCongress 2006 – Geotechnical Engineering in the Information Technology Age*, D.J. DeGroot, J.T. DeJong, J.D. Frost, and L.G. Baise (eds.), Atlanta, GA, Feb. 26 – March 1, 6 pages (electronic file).

Reinert, E.T., S.J. Brandenberg, J.P. Stewart, and R.E.S. Moss, 2013. Destructive cyclic field testing of model levee on peaty organic soil: Data report for field tests. *Report No. 2013/01*, UCLA Structural & Geotechnical Engineering Laboratory, 51 pages.

Rosco, K.H., 1953. An apparatus for the application of simple shear to soil samples, *Proc. 3rd Int. Conf. Soil Mech. Fndn. Eng.*, Vol. 1, 186-191. London: Institution of Civil Engineers.

Rutherford, C.J., 2012. Development of a multi-directional direct simple shear testing device for characterization of the cyclic shear response of marine clays, *Ph.D. Dissertation*, Texas A&M *University*.

Seed, H.B., and W.H. Peacock, 1971. The procedure for measuring soil liquefaction characteristics, *J. Soil Mech. & Foundations Div.*, 97(8), 1099-1119.

Shen, C.K., K. Sadigh, and L.R. Hermann, 1978. An analysis of NGI simple shear apparatus for cyclic load testing, *Dynamic Geotechnical Testing*, ASTM STP 654, ASTM International, West Conshohocken, PA, 148-162.

Stokoe, K.H., J.A. Bay, B.L. Rosenbald, S.K. Hwang, and M.R. Twede, 1996. In situ seismic and dynamic laboratory measurements of geotechnical materials at Queensboro Bridge and Roosevelt Island. *Geotechnical Engineering Rep. No. GR94-5*, Civil Engineering Dept., Univ. of Texas at Austin, TX.

Tatsuoka, F. and M.L. Silver, 1981. Undrained stress-strain behavior of sand under irregular loading, *Soils and Foundations*, 21(1), 51–66.

Taylor, D.W., 1978. *Fundamentals of Soil Mechanics*, John Wiley & Sons, Inc., Newyork, 700 pp.

Vaid, Y.P. and W.D.L. Finn, 1979. Static shear and liquefaction potential, *J. Geotech. Eng.*, ASCE, 105(10), 1233-1246.

Vucetic, M., G. Lanzo, and M. Doroudian, 1998. Damping at small strains in cyclic simple shear test, *J. Geotech. Geoenviron. Eng.*, 124(7), 585–594.

Wehling, T.M., R.W. Boulanger, R. Arulnathan, L.F. Harder, and M.W. Driller, 2003. Nonlinear dynamic properties of a fibrous organic soil, *J. Geotech. & Geoenv. Eng.*, 129 (10), 929-939.

Wijewickreme, D., 2010. Cyclic shear response of low plastic Fraser River silt, *Proc. 9th U.S. and 10th Canadian Conf. on Earthquake Engineering*, Toronto, Ontario, Canada, Paper No. 1431.

Yee, E., J.P. Stewart, and R.P. Schoenberg, 2011. "Characterization and utilization of noisy displacement signals from simple shear device using spectral, linear, and kernel regression, *Soil Dynamics and Earthquake Engineering*, 31 (1), 25-32.

Yee, E., P.M. Duku, and J.P. Stewart, 2013. Cyclic volumetric strain behavior of sands with fines of low plasticity, *J. Geotech. Geoenviron. Eng.*, DOI: 10.1061/(ASCE)GT.1943-5606.0001041.